REVIEW

National Science Review
4: 761–780, 2017
doi: 10.1093/nsr/nwx019
Advance access publication 24 February 2017

MATERIALS SCIENCE

Metal nanoparticles induced photocatalysis

Lequan Liu[1,2,*], Xinnan Zhang[1], Lufeng Yang[1], Liteng Ren[1], Defa Wang[1,2] and Jinhua Ye[1,2,3,*]

ABSTRACT

Photocatalysis induced by light absorption of metal nanoparticles (NPs) has emerged as a promising strategy for exploiting efficient visible-light-responsive composites for solar-energy conversion. In this review, we first introduce the light absorption of metal NPs and the mechanisms proposed in metal-induced photocatalysis (MIP). Then, its applications in water splitting, artificial photosynthesis and inert molecular activation are summarized. To address the challenge of low efficiency in this field, strategies in promoting catalytic activity are reviewed, and particular attention is paid to the particle-size effect of metal. Finally, the challenges and possible development directions of MIP are briefly discussed.

Keywords: localized surface plasmon resonance, interband transition, metal-induced photocatalysis, visible-light-responsive photocatalysis, particle-size effect of metal

[1]TU-NIMS International Collaboration Laboratory and Tianjin Key Laboratory of Composite and Functional Materials, School of Material Science and Engineering, Tianjin University, Tianjin 300072, China; [2]Collaborative Innovation Center of Chemical Science and Engineering (Tianjin), Tianjin 300072, China and [3]Environmental Remediation Materials Unit, National Institute for Materials Science (NIMS) 1-1 Namiki, Tsukuba, Ibaraki 3050044, Japan

*Corresponding authors. E-mails: Lequan.Liu@tju.edu.cn; Jinhua.Ye@nims.go.jp

Received 30 December 2016; **Revised** 26 January 2017; **Accepted** 7 February 2017

INTRODUCTION

In the past decade, there has been a surge of interest in exploring the effect of metal in photocatalysis, while attention was devoted to utilizing light absorption of metal nanoparticles (NPs) other than their conventional application as cocatalysts. Light absorption is a characteristic property of metal NPs, particularly for coinage metal (Au, Ag and Cu) NPs which are visible to the unaided eye. This property has already found applications in medical therapy, surface-enhanced Raman spectroscopy, etc. [1]. Kozuka *et al.* carried out pioneer work in metal-induced photocatalysis (MIP) by introducing Au and Ag on the TiO_2 layer in photoelectrochemical (PEC) evaluation [2]. Great advances have been achieved in this field, and MIP has become a promising strategy for developing efficient visible-light-responsive composite materials.

The total extinction cross-section of these NPs composes scattering and absorption [3]. The ratio of scattering to absorption changes dramatically with size. Large particles scatter light very efficiently, whereas the color of small particles is mainly caused by absorption. Though scattering also finds application in photocatalytic devices [4], absorption of metal NPs attracts more attention. Generally, there are two excitation models which are closely related to MIP process, namely localized surface plasmon resonance (LSPR) and interband transition. LSPR refers to light that interacts with particles much smaller than the incident wavelength, which leads to a plasmon that oscillates locally around the nanoparticle with certain frequency [5]. Though some alternative plasmonic materials (e.g. metamaterials) have been developed [6], plasmons of metal is still the main research subject in plasmonic photocatalysis. Furthermore, coinage metals account for the main part in this field. Another critical absorption model of metal is interband transition due to transitions between deeper bands (e.g. the d-bands of noble metals) and the conduction band (CB). Among transition metals, coinage metal NPs generally possess characteristic LSPR absorption in or near the visible-light region. Nevertheless, it is still a matter of debate that absorption in the ultraviolet-visible range of the other metals is attributed to LSPR or interband transitions [7]. On the other hand, it should be pointed out that turning the morphology or increasing particle size to hundreds of nanometers can induce non-coinage metals to exhibit resolved LSPR absorption [8,9]. From this perspective, these absorptions of non-coinage metals may also be regarded as LSPR in a broad sense. For LSPR, the population decay occurs via transformation of particle plasmons into photons (radiation damping) and via nonradiative decay into electron–hole excitations Fig. 1 [10]. The

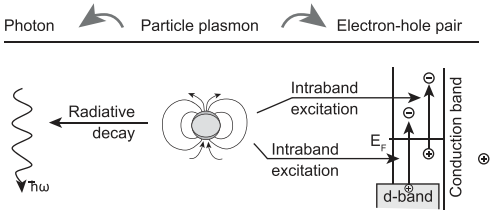

Figure 1. Schematic representation of radiative (left) and nonradiative (right) decay of particle plasmons in noble-metal NPs. The nonradiative decay occurs via excitation of electron–hole pairs either within the conduction band (intraband excitation) or between the d-band and the conduction band (interband excitation) [10]. Reprinted with permission from Ref. [10]. Copyright 2002, by the American Physical Society.

latter fall into two categories: intraband excitations within the CB and interband excitations. Generally, radiative damping is the dominant decay for large NPs (e.g. larger than 50 nm for dipolar plasmon resonances), while nonradiative damping is the dominant decay mechanism for small NPs [11].

Various applications such as dye degradation, organic pollutant removal, fine chemical synthesis, water splitting, CO_2 photoreduction, etc. have been found to be induced by light absorption of transition metals, in particular for visible-light response. More specifically, roles played by these metals in photocatalysis can be generally divided into: activity enhancement, photosensitization of semiconductors, solely LSPR catalysis, photothermal effect, light-trapping effect, etc. Among all these MIP systems, the photosensitization effect arouses particular interest because it offers a novel approach to overcoming the photo-absorption limitation of semiconductors with large band-gaps (e.g. >3.0 eV). MIP has been proved to be a promising strategy in developing efficient visible-light-responsive photocatalysts, while the research and development in this field are still at a relatively early and fundamental stage. Achieving efficient metal-induced visible-light photocatalysis still remains a big challenge in this field. Further efforts are urgent to get deeper insight into underlying mechanisms and to improve their performance. This review will summarize the main recent achievements in this field from the perspective of the mechanism, MIP applications in water splitting, artificial photosynthesis and inert molecular activation. To address the challenge of low efficiency in this field, strategies in promoting catalytic activity are summarized, and particular attention is paid on the particle-size effect of metal.

MECHANISM OF ENERGY TRANSFER FROM METAL TO SEMICONDUCTORS

Hot-electron transfer

This mechanism was first proposed by Tatsuma's group in explaining the observed enhanced incident photon-to-current conversion efficiency (IPCE) under visible-light illumination by loading Au or Ag NPs into TiO_2 films [12,13]. As shown schematically in Fig. 2, plasmon-resonance-excited electrons were proposed to transfer from Au or Ag to the CB of adjacent TiO_2. This mechanism is similar to that of a dye-sensitized solar cell. Direct electron transfer from excited metal to semiconductors is supported by more and more experimental observations in recent years. Pioneer work was carried out by Furube and co-authors, in which electron transfer from Au to TiO_2 was confirmed by femtosecond transient absorption spectroscopy investigation [14]. Recently, Tatsuma *et al.* studied the charge distributions for Au nanoparticles deposited on crystalline TiO_2 by in-situ Kelvin probe force microscopy [15]. A positive shift of surface potential difference (E_{Au}–E_{TiO2}) was observed when the composite material was excited with visible and

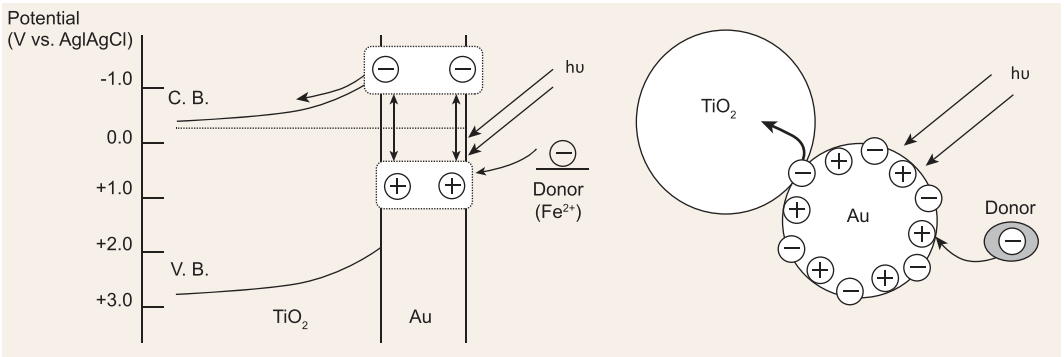

Figure 2. Proposed mechanism for the photoelectrochemistry: charges are separated at a visible-light-irradiated Au NPs—TiO_2 system [13]. Reprinted with permission from Ref. [13]. Copyright 2005, by the American Chemical Society.

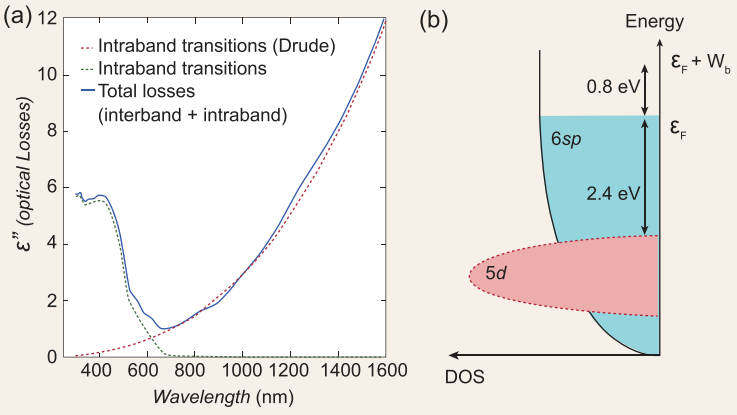

Figure 3. (a) Imaginary permittivity or optical losses in gold [6]. Reprinted with permission from Ref. [6]. Copyright 2013 by WILEY-VCH, Weinheim. (b) Band structure of gold, Fermi energy ε_F [25]. Reprinted with permission from Ref. [25]. Copyright 2015, by the American Chemical Society.

near-infrared (NIR) light, indicating electron injection from the resonant Au NPs to TiO_2, as opposed to the case of excitation by UV light. Electron transfer was also studied in Au and perovskite $CH_3NH_3PbI_3$ composites by plasmon resonance Rayleigh scattering spectroscopy [16]. Furthermore, 'hot' electron injection from Au to semiconductor has been utilized for photo-detection devices, in which the light-harvesting spectral range was greatly extended [17].

Though the transfer process is experimentally confirmed, the source of charge carriers excited in metal is still a subject of debate. For example, the light absorption of Au comprises two models, i.e. LSPR and interband transition, as shown in Fig. 3a. At the early stage, it is generally accepted that hot electrons should come from LSPR. However, as plasmonic charge resides in the Fermi energy of the metal, it raises doubts on whether these plasmonic charge carriers are able to drive the reduction and oxidation half reactions [18]. As hot electrons transfer to the CB of semiconductors with certain reductive potential, particular attention should be paid to the potentials of the leaving holes in metals. Compared with plasmon resonance, interband transition generally requires higher photon energy to excite electrons from deeper bands (e.g. the d-bands of gold) (Fig. 3b). That is, photo-generated holes in the interband transition are created far from the Fermi surface. These assumption finds support from theoretical study on the redox potentials of charge carriers generated in LSPR and interband transition carried out by Govorov and co-workers [19]. In our recent work, symmetrical study reveals that Au interband transitions offer the main driving force for photocatalytic water oxidation over $Au/SrTiO_3$ [20,21]. Similar conclusions were also reached in photocatalytic organic reactions or degradation over Pt, Pd, Rh and Ir [22,23]. On the other hand, it should be pointed out that the source of hot electrons is not exclusive. Bruckner and co-authors demonstrated that both plasmon resonance and interband transitions were involved in visible-light water reduction by in-situ electron paramagnetic resonance (EPR) spectroscopy study [24].

Near-field enhancement

In addition to the hot-electron transfer mechanism, near-field enhancement is another important mechanism in MIP. It has been demonstrated that the electron–hole formation rate in semiconductors is proportional to the local intensity of the electric field [26]. Photo-excited plasmonic nanostructures can generate intense local electric fields near the surface, and the strength of these fields is generally orders of magnitude higher than the field of photons used to photo-excite the metallic nanostructures. The near-field electromagnetic mechanism is based on the interaction of semiconductor with the strong LSPR-induced electromagnetic fields in the vicinity of plasmonic metals. On the other hand, these fields are spatially non-homogenous, and decrease exponentially with the distance from the metallic nanostructure to the semiconductor. This feature was experimentally demonstrated by a designed $Au@SiO_2/CdS$ nanostructure where the semiconductor and the plasmonic metal were separated from each other by a thin insulator, preventing any direct electron transfer [27]. The activity varied with different distances between Au and CdS by adjusting the thickness of the SiO_2 layers. This mechanism also finds support in other systems [28–30].

Another alternative mode of near-field enhancement is plasmon-induced resonance energy transfer (PIRET), which was proposed by Wu and co-workers [31,32]. This mechanism originates from the dipole–dipole coupling between plasmon and semiconductor interband transition. Experimental results observed for $Ag@Cu_2O$, $Au@Cu_2O$, $Au@SiO_2@Cu_2O$ and $Ag@SiO_2@TiO_2$ nanoparticles in photocatalysis applications were successfully explained with this mechanism [31,33–35] As stated above, the LSPR-mediated electromagnetic field accelerates the electron–hole pair generation using incident energies above the semiconductor's band-gap. For the PIRET mechanism, however, the electron–hole pairs in the semiconductor are claimed to be excited through the relaxation of the localized surface plasmon dipole, at energies both above and below the semiconductor's band-gap. The strength of PIRET depends on the overlap of the

semiconductor's band edge with the LSPR resonance band, as well as the distance between the plasmonic metal dipole and the semiconductor dipole.

Besides the popular mechanisms stated above, there may exist other energy-transfer pathways played by plasmonic metals [36]. For example, light trapping has been proven to be an effective method for increasing photo-conversion in semiconductor film photovoltaics [4,37]. Moreover, recent study indicates that energetic electrons excited by LSPR facilitate the polarization and activation of inert gases such as CO_2, CH_4 and N_2 [38,39]. Furthermore, the heating effect that originates from the radiative decay of plasmons can serve as a straightforward and effective method in the utilization of a wide range of solar spectra for the photothermal conversion of CO_2 [40]. Detailed explanation will be given in subsequent sections.

METAL-INDUCED VISIBLE-LIGHT PHOTOCATALYSIS

The integration of plasmonic metal NPs with semiconductors results in the formation of metal semiconductor composite (MSC) materials with enhanced solar-light-harvesting ability. This provides a potential solution for the well-recognized challenge in the solar-energy conversion field, i.e. visible, even NIR light response. A vast majority of work has been carried out on its applications. In the following section, we focus on the progress towards MIP applications in photocatalytic and PEC water splitting, photoreduction of CO_2 and plasmonic activation of inert moleculars such as CH_4, N_2. Other applications, including sole plasmonic photocatalysis, decomposition of organic compounds and organic reactions, readers can refer to some excellent reviews on these subjects [41–47].

Solar-water splitting

Owing to the challenges from environment pollution and the energy crisis that we are facing, a revolution towards clean and renewable energy has been set off. In all of the new energy resources, hydrogen is one of the most attractive fuels for production because of its high energy capacity and environmental friendliness. Since PEC water splitting over TiO_2 was first demonstrated by Fujishima and Honda in the 1970s, it has attracted enormous attention due to its great potential for resolving environmental and energy issues [48]. By depositing plasmonic metal NPs, semiconductors such as TiO_2 have been demonstrated to be visible-light-responsive in both photocatalytic and PEC water splitting [2,20,49–52]. This photosensitization effect offers a promising strategy in overcoming the absorption energy limitation of semiconductors. One could achieve photocatalytic hydrogen and oxygen evolutions under either polychromatic light $\lambda > 400$ nm or monochromatic 532-nm laser excitation over Au/TiO_2 (Fig. 4a) [49]. In contrast, a negligible amount of hydrogen was produced with TiO_2 only. The observed photocatalytic activity was ascribed to the electron transfer from Au NPs to TiO_2. In our previous work, a remarkable O_2 evolution rate comparable to commercial WO_3 was achieved over $Au/SrTiO_3$ under visible-light irradiation (Fig. 4b) [20]. Although $SrTiO_3$ and TiO_2 possess similar band structures, $Au/SrTiO_3$ exhibited superior activity, indicating that a band match issue may exist between Au and semiconductors. In addition to composite materials, plasmonic metal solely was also demonstrated to drive visible-light water splitting. Pt-modified Au nanorods (NRs) synthesized by anisotropic overgrowth showed H_2 evolution activity under visible and NIR light irradiation, though the efficiency is relatively low (Fig. 4c) [53]. A similar strategy was also adopted by other groups [54].

Another important aspect in utilizing metal absorption in water splitting is photocatalytic enhancement, in particular for PEC study. In an early report, Kamat *et al.* improved the PEC performance of TiO_2 films by modification with Au NPs; a three-fold enhancement in photocurrent generation has been achieved [55]. The improved PEC performance was explained on the basis of improved interfacial charge-transfer kinetics. Cronin *et al.* reported even higher enhancement factors of 5 and 66 at 532 nm and 633 nm, respectively, in the water-splitting reaction under visible-light illumination by depositing Au NPs on the top of anodic TiO_2 with defect states (Fig. 4d) [56]. It is claimed that local electric field enhancement near the TiO_2 surface increases the electron–hole pair generation rate. It is generally accepted that a strong electromagnetic field accompanied by LSPR plays an important role in enhancement effect. On the other hand, the field is spatially non-homogeneous and decays exponentially with distance. So, nanostructure designing is an important factor which should be taken into account in developing efficient MIP systems. Thomann *et al.* reported plasmon-enhanced photocatalytic water splitting on Fe_2O_3 films with $Au@SiO_2$ that were either embedded in or on the top of the Fe_2O_3 surface (Fig. 4e and 4f) [30]. The highest photocurrent enhancement, 11-fold at 590 nm, was observed in the particle-on-top configuration. The enhanced performance was ascribed to plasmon-enhanced light absorption on comparison of spectral features in the enhanced photocurrent

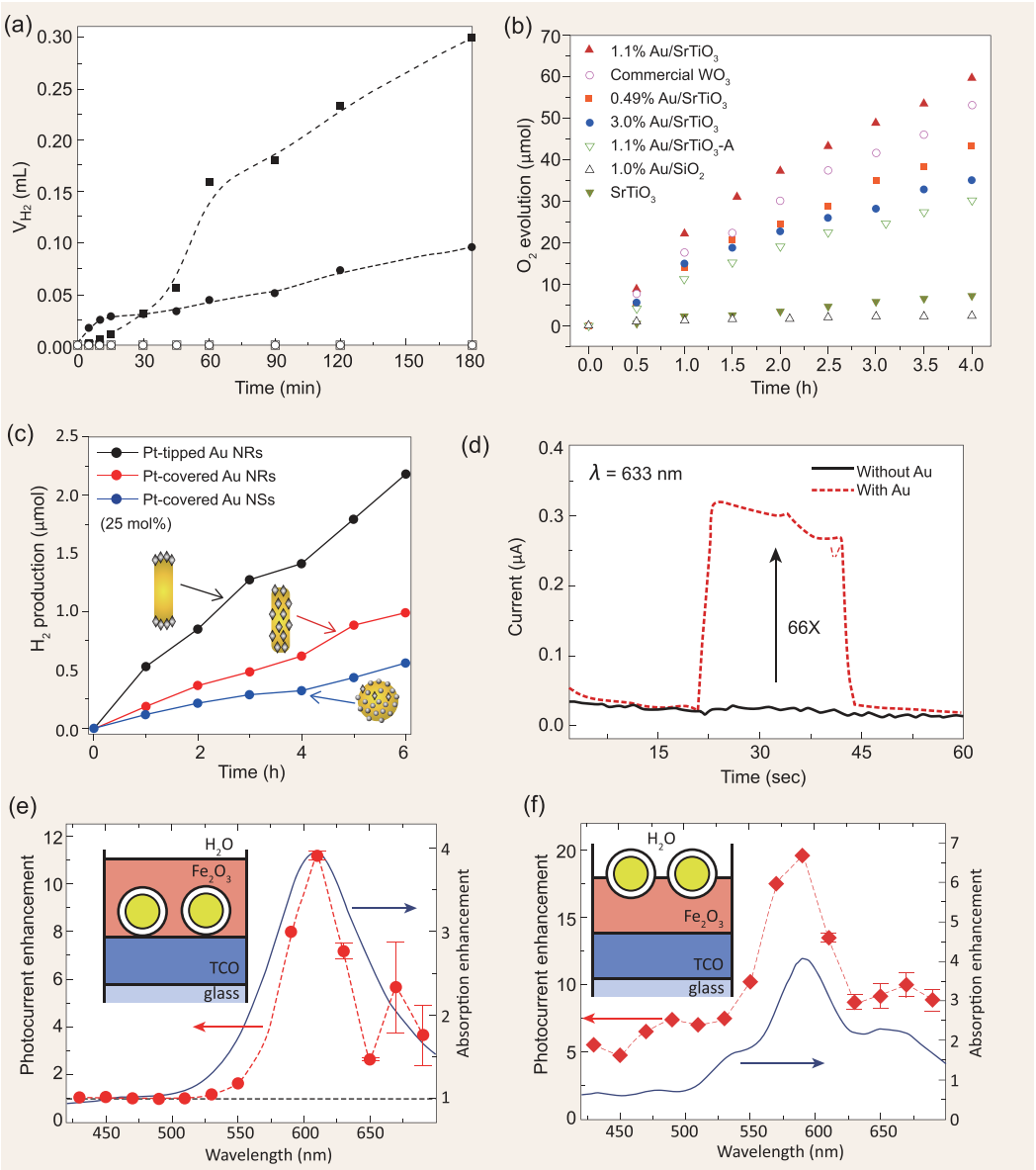

Figure 4. (a) Volume of hydrogen evolved during the photocatalytic runs using TiO_2 and Au (1.5 wt %)/TiO_2 as catalysts and Ethylenediaminetetraacetic acid (EDTA) as sacrificial electron donor, under 532-nm laser irradiation and polychromatic light $\lambda > 400$ nm. ■: Au/TiO_2, $\lambda = 532$ nm; •: Au/TiO_2, $\lambda > 400$ nm;◯: TiO_2, $\lambda = 532$ nm; □: TiO_2, $\lambda > 400$ nm [49]. Reprinted with permission from Ref. [49]. Copyright 2011, by the American Chemical Society. (b) Curves of O_2 evolution as a function of reaction time under visible-light irradiation ($\lambda > 400$ nm). Reaction conditions: 0.2 g catalyst, 5 mmol $AgNO_3$, 300-W Xe lamp [20]. Adapted with permission. Copyright 2014, by The Royal Society of Chemistry. (c) Time course of H_2 evolution from water—methanol (20 vol %) suspensions of Pt-modified Au NPs (0.188 mg) under visible-light irradiation ($460 < \lambda < 820$ nm) [53]. Reprinted with permission from Ref. [53]. Copyright 2014, by the American Chemical Society. (d) Photocurrent of anodic TiO_2 with and without Au NPs irradiated with $\lambda = 633$ nm light for 22 s [56]. Reprinted with permission from Ref. [56]. Copyright 2011, by the American Chemical Society. (e, f) Photocurrent enhancement spectra for Au NPs with a silica shell. Measured photocurrent (red symbols) and simulated (solid blue lines) absorption enhancement spectra that show the beneficial effects of placing silica-coated Au NPs at the bottom (e)/on top (f) of a 100-nm thin Fe_2O_3 photoelectrode layer [30]. Reprinted with permission from Ref. [30]. Copyright 2011, by the American Chemical Society.

spectra to full-field electromagnetic simulations. In another case, a sandwich-structured CdS-Au-TiO_2 nanorod array as the photoanode in a PEC cell for hydrogen generation was synthesized [57]. The Au NPs sandwiched between TiO_2 nanorod and CdS quantum dot (QD) layer have a dual function in enhancing the solar-to-chemical energy-conversion efficiency. First, Au NPs facilitate the charge transfer between CdS and TiO_2. Second, Au NPs enable the reaction at wavelengths longer

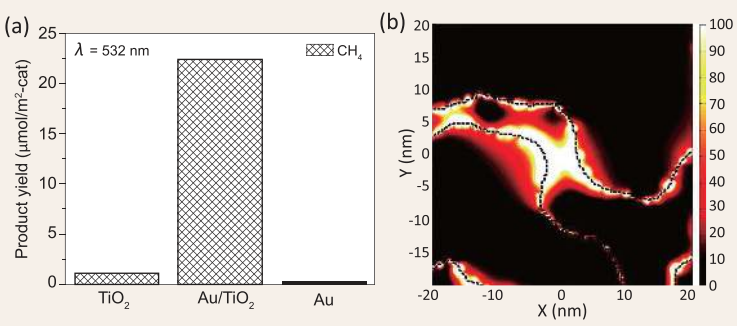

Figure 5. (a) Photocatalytic product yields (after 15 h of visible-light irradiation) on three different catalytic surfaces. (b) Electric-field intensity at the interface of Au–TiO_2 calculated using the finite-difference time-domain (FDTD) method [65]. Reprinted with permission from Ref. [65]. Copyright 2011, by the American Chemical Society.

than the band edge of CdS and even extend the photo-conversion wavelength from 525 to 725 nm. Upon full solar spectrum irradiation, this PEC cell can achieve a photocurrent of 4.07 mA/cm^2 at 0 V vs. Ag/AgCl and maximum solar-to-chemical energy conversion efficiency of 2.8%. Similar enhancement was also reported by other groups [58,59]. Though a number of achievements have been achieved in this field, the research is still in its early stage. Effort is highly needed to enhance the efficiency of H_2 or O_2 evolution induced by light absorption of metal NPs. Various strategies developed on this subject will be reviewed in the 'Several ways to promote the efficiency of MIP' section.

CO_2 photoreduction

The photocatalytic reduction of CO_2 to hydrocarbon fuels, which is artificially converting solar energy into fuels to solve the problems of energy shortage as well as the greenhouse effect of CO_2, attracts great interest. Pioneering work on photocatalytic CO_2 reduction was conducted by Halmann in 1978, in which HCOOH, HCHO and CH_3OH was obtained over a p-type GaP electrode [60]. In 1979, Inoue *et al.* also demonstrated that CO_2 could be photoelectrically reduced into organic compounds by using various semiconducting photocatalysts [61]. From then on, various types of semiconductors have been reported in the field of CO_2 photoreduction [62–64]. Although these efforts have yielded excellent results, which demonstrated the feasibility of photocatalytic CO_2 reduction to useful chemical products, they still faced a big challenge in activating CO_2. Hot electrons and LSPR induced electromagnetic-field of metal NPs offer a potential pathway for CO_2 photoreduction.

Similarly to the enhancement stated above, one can expect that the incorporation of plasmonic metal can enhance the light absorption of MSC materials and promote the photoreduction of CO_2. Cronin *et al.* reported that quantum efficiency could be improved by a factor of 24 over Au-deposited TiO_2 film as compared with pure TiO_2 under visible irradiation (532 nm) (Fig. 5a) [65]. The promoting effect was attributed to the prominently enhanced electron–hole pair excitation rate due to LSPR-induced strong electric fields (Fig. 5b). This attribution is mainly based on electromagnetic field simulation. Incorporating cocatalysts can further improve the catalytic performance. For example, Xue *et al.* prepared TiO_2 nanofibers decorated with Au, Pt NPs and investigated the photoreduction of CO_2 to CH_4 under UV–vis irradiation [66]. It was found that AuPt/TiO_2 exhibited a 1.8-fold and 1.4-fold higher CH_4 production compared to Au/TiO_2 and Pt/TiO_2, respectively. The higher activity was attributed to the improved charge-carrier separation induced by the LSPR effect of Au and the Pt NPs as electron sinks and reduction sites. In addition to the enhancement effect, LSPR was also demonstrated to modulate the selectivity in CO_2 photoreduction. Reduced graphene-coated Au NP (r-GO-AuNPs)-TiO_2 hybrid photocatalysts were demonstrated to effectively convert CO_2 into HCOOH [67]. The hybrid material (quantum yield: 1.52%) showed excellent selectivity for HCOOH (>90%) and higher conversion efficiency than Pt-coated Au NPs-TiO_2 hybrid material (quantum yield: 1.14%). Zhou and Zou *et al.* prepared an Au@TiO_2 yolk–shell hollow sphere [68]. An LSPR-mediated electromagnetic field near to Au nanoparticles is claimed not only to enhance the local generation and subsequent separation of e^-–h^+ pairs in TiO_2 shells to improve the yield of photoreduction CO_2, but also to facilitate chemical reactions involving multiple e^-/h^+ transfer processes to allow the formation of high-quality carbon species (C_2H_6), which was rarely observed in present CO_2 photocatalytic-reduction systems. These results provide a novel way in developing efficient MSC materials for CO_2 photoreduction, which could inspire future work in this area.

Another perspective of promoting CO_2 photoreduction is facilitating its activation under mild conditions. The interaction between light (electric field) and plasmonic metal NPs through LSPR induces the formation of hot electrons and dipoles with inhomogeneous distribution, which potentially excite or polarize nonpolar molecules for activation. This capability offers another important application in the photoreduction of CO_2, i.e. activation of inert nonpolar reactants by using light. Halas *et al.* demonstrated a good example of room-temperature dissociation of H_2 over Au NPs using visible light [69]. Surface plasmons excited in the Au NPs decay into hot electrons with energies between the

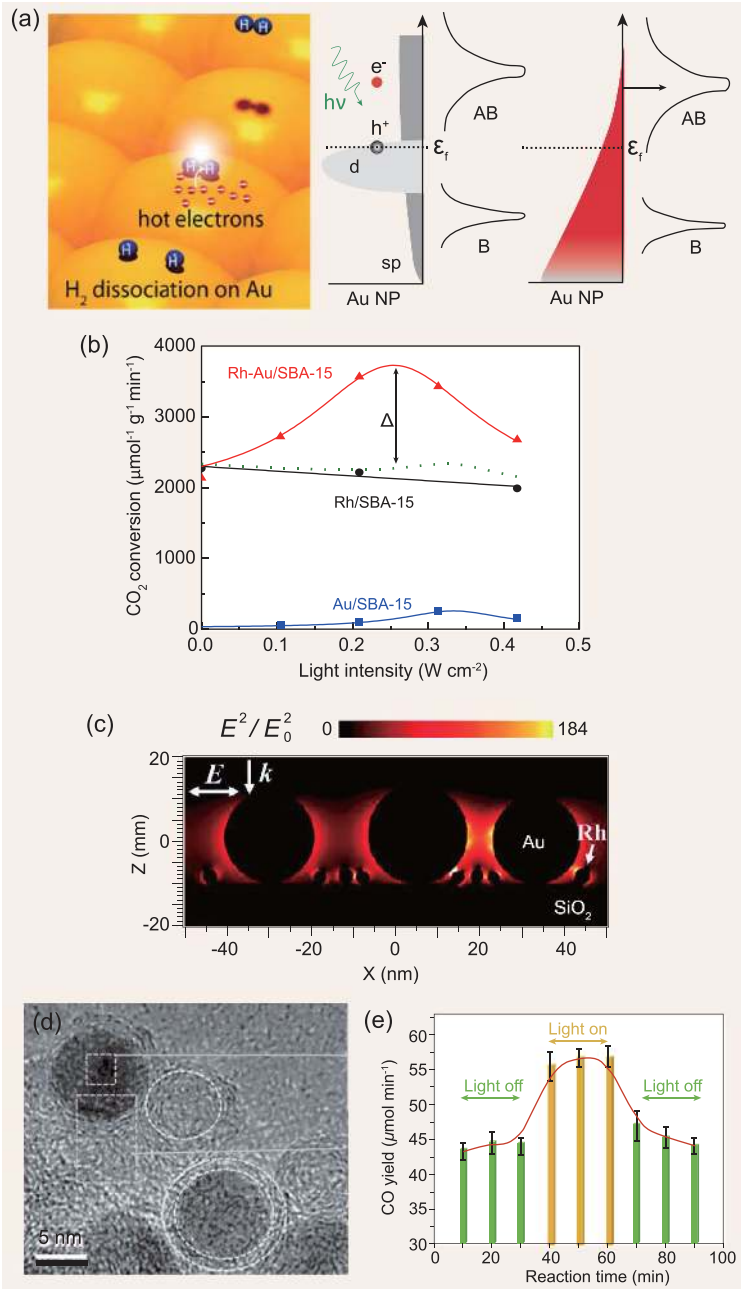

Figure 6. (a) Left: schematic illustration of the proposed mechanism; middle: schematic of hot-electron excitation in Au NP showing: d-band electron—hole pair excited above the Fermi level upon plasmon decay. The narrow bonding and broad anti-bonding states of adsorbed H_2 are denoted as B and AB, respectively; right: schematic of Fermi—Dirac type distribution of hot electrons permitting hot-electron transfer into the anti-bonding state of H_2 [69]. Reprinted with permission from Ref. [69]. Copyright 2013, by the American Chemical Society. (b) Effects of visible-light intensities on CO_2 methane reforming into syngas. (c) Cross-sectional views of the electromagnetic field distribution and enhancement in Rh-Au/SBA-15 simulated with the FDTD method [38]. Reprinted with permission from Ref. [38]. Copyright 2015, by WILEY-VCH, Weinheim. (d) HRTEM images of the hybrid, showing the carbon shells and encapsulated Fe NPs. (e) CO-evolution rates at 450°C with and without UV-light illumination over Fe@C catalyst. A significant enhancement in the reaction rate caused by UV-light illumination was observed [39]. Reprinted with permission from Ref. [39]. Copyright 2016, by WILEY-VCH, Weinheim.

vacuum level and the work function of the metal. In this transient state, hot electrons can transfer into a Feshbach resonance of an H_2 molecule adsorbed on Au surface, and trigger dissociation as shown in Fig. 6a. Such a strategy was further developed by Ye and co-workers to promote CO_2 activation [70]. It was demonstrated that Au enhanced the catalytic performance of Rh/SBA-15 in reforming CO_2 with methane under visible-light irradiation (CO_2 conversion increased from 2100 to 3600 μmol/g/s), while Au was regarded to be inactive in improving the performance of this reaction under thermal conditions (Fig. 6b). Electromagnetic field simulation suggested that the highly energetic electrons excited by LSPR of Au facilitated the polarization and activation of CO_2 as well as CH_4 with thermal assistance (Fig. 6c). In a further study, PdAu alloy as catalysts was found not only to favor the stability of the Pd_xAu_y/Al_2O_3 catalysts in thermal-driven CO_2 reduction, but also to facilitate CO_2 activation by electromagnetic field and hot electrons induced by plasmonic absorption in visible-light region [71]. Recently, MOF-derived Fe@C catalyst composed of an iron core <10 nm and ultrathin carbon layers was investigated in the solar-driven photoreduction of CO_2 to CO (Fig. 6d) [72]. In comparison with naked iron particles, the carbon-layer-coated catalysts exhibited improved catalytic performance in the solar-driven CO_2 conversion by H_2 and a higher selectivity to CO (Fig. 6e). Field-simulation results indicated that the plasmon–photon coupling was largely amplified on the surface of iron particles, leading to the enhanced generation of energetic hot electrons for CO_2 activation.

As stated above, the energy of LSPR can be transformed into heat through radiative decay, and this heating effect may be so prominent that it can drive thermocatalysis. Ye *et al.* took full advantage of the plasmonic-induced photothermal effect based on Group VIII metals (Ru, Rh, Ni, Co, Pd, Pt, Ir and Fe) for the catalytic conversion of CO_2 with H_2 into CH_4 and CO for the highly efficient production of solar fuels [73]. It suggests that reaction rates for the photothermal CO_2 conversion could be enhanced strongly due to several features of the Group VIII nanocatalysts, including effective energy utilization, excellent photothermal performance and a unique H_2-activation ability. A similar phenomenon was also observed by Ozin *et al.* over Ru/Silicon nanowire catalysts with visible and NIR photons in CO_2 photomethanation [64]. Although using plasmonic photocatalysts for CO_2 reduction has gained great interest and shown progress during the last few years, further effort should be made on this subject in particular for designing an efficient CO_2

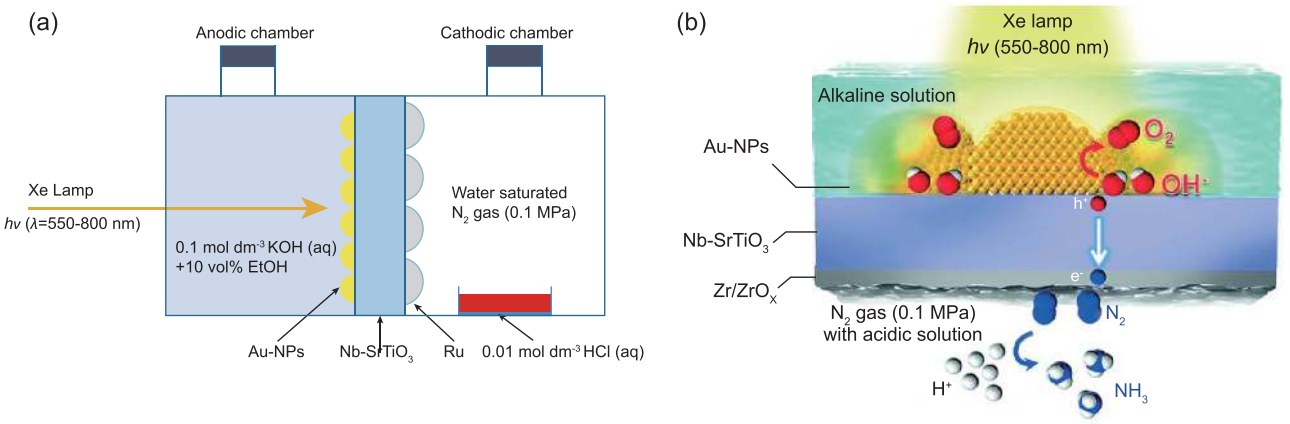

Figure 7. (a) A schematic illustration of the NH_3 synthesis device using a Nb-$SrTiO_3$ photoelectrode loaded with Au NPs [79]. Reprinted with permission from Ref. [79]. Copyright 2014, by WILEY-VCH, Weinheim. (b) Layout of the NH_3 synthesis device bearing the Nb-$SrTiO_3$ photoelectrode loaded with Au NPs and a Zr/ZrO_x thin film [80]. Reprinted with permission from Ref. [80]. Copyright 2016, by WILEY-VCH, Weinheim.

photoreduction system carried out under relatively mild conditions.

Activation of inert molecules such as N_2 and CH_4

In the past decades, photocatalytic N_2-fixation technology has become one of the best alternatives to traditional industrial N_2-fixation techniques due to its advantages of green cleaning and mild reaction conditions, among others. In 1977, Schrauzer *et al.* first reported that N_2 can be reduced to NH_3 over Fe-doped TiO_2 under UV light [74]. Thereafter, various efforts have been made on photocatalytic N_2 reduction to NH_3 [75–77]. More recently, oxygen vacancies of BiOBr nanosheets have been investigated for N_2 reduction [78]. However, due to the high stability of N_2, the efficiency is generally low, which is still a big challenge. As a possible approach to overcoming this problem, researchers have attempted to exploit the potential of plasmonic metal in its activation. Misawa's group carried out some pioneer work in this field. For instance, plasmon-induced NH_3 synthesis has been demonstrated on a Au NP-coated Nb-$SrTiO_3$ substrate with visible-light irradiation [79]. A chemical bias was applied to promote NH_3 formation, and its formation action spectrum was highly consistent with the LSPR band (Fig. 7a). Plasmon-induced charge separation at the Au/$SrTiO_3$ interface promoted oxidation at the anodic chamber and subsequent nitrogen reduction on the cathodic side. They also reported a highly selective and visible-light-responsive plasmonic NH_3 synthesis device containing an Au nanostructure and a Zr/ZrO_x thin film (Fig. 7b) [80]. N_2 was reduced to NH_3 using water as an electron donor under visible-light irradiation. Through density functional theory, Martirez *et al.* gave out some useful guidance for N_2 activation by using AuM (M = Fe, Co, Ni and Mo) alloy [81]. Both the reactivity towards N_2 and the ability to support a pathway for N_2 dissociation with a low thermodynamic barrier were taken into account. Their results show that AuFe alloy possesses appealing qualities. In a recent study carried out by MacFarlane and Zhang *et al.*, ammonia-producing yields reached 13.3 $mg/m^2/h$ in the conversion of atmospheric N_2 under 2 suns illumination [82]. The solar-driven nanostructured PEC cell was designed based on plasmon-enhanced black silicon. Though the efficiency is still low for practical ammonia manufacture, this PEC performance shows the possibility of mimicking the nitrogen-fixation and conversion process of nitrogenases in nature.

CH_4 is a highly stable hydrocarbon with a wide distribution in nature. Due to its abundance, it could provide a new alternative in the field of fuels and chemicals [83]. Various efforts have been made to convert CH_4 to more useful chemicals and hydrogen. However, due to its stability, high energy is usually consumed for its conversion. As a possible approach to overcoming this problem, researchers have attempted to exploit the potential of introducing plasmonic metal in its activation. Yi *et al.* reported the photocatalytic oxidation of CH_4 over Ag-decorated ZnO nanocatalysts [84]. They showed that, when the particle size of ZnO is reduced down to the nanoscale, it exhibits high activity for CH_4 oxidation under simulated sunlight illumination, and nano Ag decoration further enhances the photocatalytic activity via LSPR effect. The high quantum yield of 8% at wavelengths <400 nm and over 0.1% at wavelengths about 470 nm were achieved on the Ag-decorated ZnO nanostructures, showing

great promise for atmospheric CH_4 oxidation. The prospect of using solar-light energy to activate N_2 and CH_4 is highly attractive. MSC materials engineering for the creation of highly active photocatalysts operated under ambient conditions is of great interest and deserves further study.

SEVERAL WAYS TO PROMOTE THE EFFICIENCY OF MIP

Generally, the efficiency of photocatalytic reaction is related to the absorption of light, the separation and migration of electron–hole pairs and the chemical reaction on the catalyst surface [85]. As a result, photocatalytic efficiency can be enhanced by increasing the effective photon absorption, promoting charge separation and creating more active sites. However, the case for MIP system is more complicated. Although much effort has been devoted to developing MSC materials, their efficiencies under visible-light irradiation are still low, in particular for photosensitization in harsh reactions such as photocatalytic water splitting. Several attempts have been made in studying the theoretical maximum efficiency of these MSC materials. According to the results from Thomas P. White *et al.*, the maximum efficiency limit for photovoltaics using plasmonic nanostructures was 8%, even with perfect optical absorption [86]. This limit was due to the fundamental electronic properties of metallic absorbers. However, they also pointed out that the limit could be broken by modifying the electron-density states of the absorber. By this approach, the efficiency could increase to >20%. Similar results were also obtained by other groups [87,88]. From the experimental side, relatively high efficiency may be obtained in PEC evaluation under visible-light irradiation. For example, IPCE was claimed to reach 26% over Au/TiO_2 at about 560 nm with the assistance of 4-nitrobenzoic acid to suppresses charge-carrier recombination [13]. However, for most present metal-induced photocatalytic water-splitting under visible light, the obtained apparent quantum efficiency (AQE) is relatively low (i.e. <1%) [20,21,53,54]. It has become one of the biggest challenges faced by researchers in this field. So, we have a great development space for improving the efficiencies of MSC photocatalysts. Fortunately, it has raised more and more attention, and much effort has been made. Various strategies, including morphology control, nanostructure construction and cocatalyst decoration, have been demonstrated to be effective [89–92]. In the subsequent section, efforts are devoted to summarizing achievements in developing efficient MSC materials with visible-light response, and attempts to reveal the relationship between those factors and photocatalytic efficiency are made.

Achieving broadband or effective light-harvesting

From the perspective of solar energy, it is undoubtedly important to harvesting longer-wavelength visible light, which is also applicable to plasmonic photocatalysis. Morphology-dependent LSPR absorption offers a good opportunity for harvesting longer-wavelength visible light through morphology control. For instance, LSPR absorption splits into two modes for Au NRs, corresponding to the oscillation of the free electrons along and perpendicular to the long axis [93]. That is, Au NRs possess not only a transverse mode with resonance at about 520 nm, but also a longitudinal resonance mode whose frequency strongly depends on the aspect ratio. Moreover, the absorption intensity of the longitudinal resonance mode centered at long-wavelength is generally stronger than that of the transverse mode in Au NRs, which makes the former more promising. This strategy has been adopted in our previous work by introducing Au NRs as 'antennas' over TiO_2 [94]. Broadband visible-light harvesting was achieved based on LSPR by controlling the aspect ratio of Au NRs (Fig. 8a). Meanwhile, an $HClO_4$ oxidative method was developed to remove the surfactant around Au NRs without noticeably changing its morphology. It was found that, not only transversal plasma, which is similar to sphere Au particles, but also longitudinal plasma of Au NRs could induce photocatalytic oxidation of iso-propanol (IPA) over Au NR/TiO_2 (see Fig. 8b), which extends the light-harvesting to the NIR region. A similar strategy was also adopted by other groups, and participation of longitudinal plasma was further confirmed [53,54,95,96]. In addition to Au NR, Au nanocages with hollow interiors and porous walls were also demonstrated to be effective in harvesting broadband visible light (Fig. 8c) [97,98]. Electromagnetic field simulation suggested that the plasmon–photon coupling effect was dramatically amplified at the interface between the Au NR and C–TiO_2, leading to enhanced generation of energetic hot electrons for photocatalysis (Fig. 8d). From different literature, it is generally difficult to compare the enhancement or photosensitization effect of metal with different morphologies. A study from Gołąbiewska *et al.* offers a chance to get insight into the influence of morphology in MIP [99]. For photocatalytic aqueous phenol degradation under visible light, an amorphous form of a TiO_2 sample modified by spherical

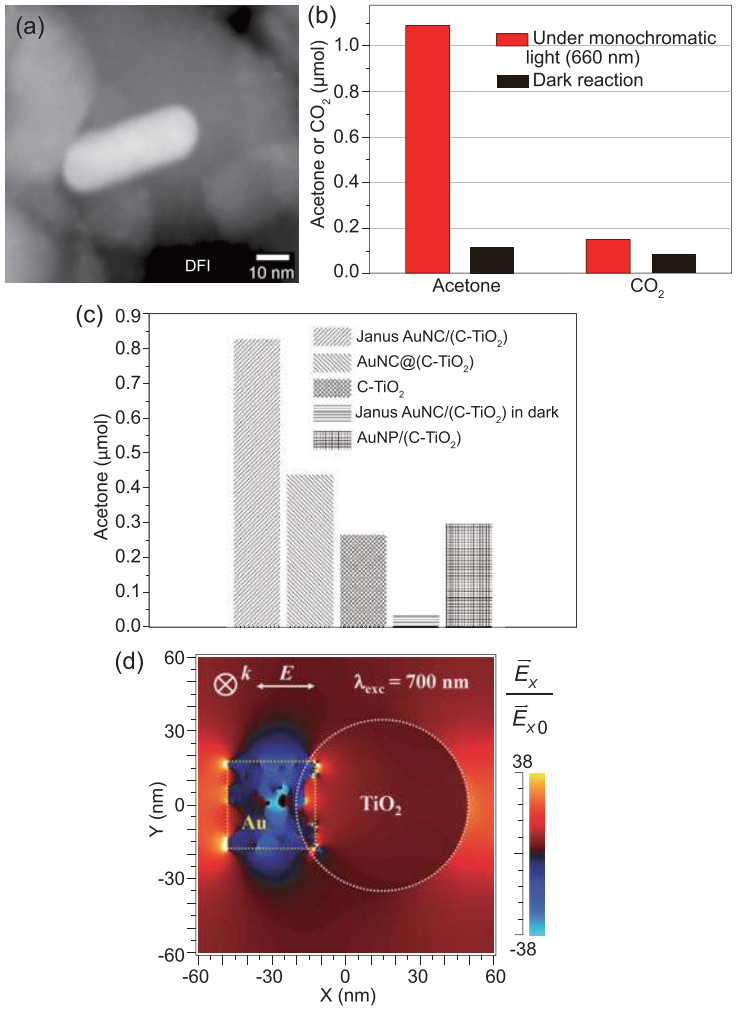

Figure 8. (a) HAADF-STEM image and (b) acetone or CO_2 evolution over Au NR/TiO_2 photocatalyst [94]. Reprinted with permission from Ref. [94]. Copyright 2013, by WILEY-VCH, Weinheim. (c) Acetone evolution from the photocatalytic oxidation of IPA over various photocatalysts carried out under monochromatic light (709 nm) irradiation for 13.5 h. (d) Electromagnetic field distribution and enhancement simulated with the FDTD method. Simulated electric field distribution: E_x normalized to the incident field E_{x0}. The excitation wavelength, λ_{exc}, was 700 nm; *k* indicates the wave-vector; the color scale bar shows the electric field enhancement, E_x/E_{x0}, with the negative and positive electric field amplitudes [97]. Reprinted with permission from Ref. [97]. Copyright 2014, by WILEY-VCH, Weinheim.

particles of gold exhibited the highest activity. According to their result, the visible-light activity decreased in the following order: nanospheres > nanorods > nanostars.

Effective visible-light harvesting is not limited to LSPR; interband transitions of metal is another crucial factor which should be taken into account in particular for metal-induced harsh photocatalytic processes. Compared with Au, Cu possesses a lower interband transition threshold of 1.9 eV, so it should be more efficient in driving visible-light photocatalytic water splitting if interband transition offers the main driving force. However, the easy oxidation property restricts its application. Recently, we demonstrated that visible-light H_2-evolution activity over Au-Cu alloy/$SrTiO_3$ was obviously enhanced as compared with Au/$SrTiO_3$ or Cu/$SrTiO_3$ by introducing Cu with Au to form an alloy [21]. These results not only confirm the proposition that the interband transition of Au offers the main driving force for visible-light photocatalytic water splitting over Au or Cu/$SrTiO_3$, but also offer a novel way of promoting the efficiency of an MIP system.

Enhancing charge-carrier separation

The lifetime of hot electrons in plasmonic NPs is less than 10^{-3} ns. For Au/TiO_2 composites without an electron donor, the injected hot electrons to TiO_2 may decay back to the Au plasmonic NPs just after ~1.5 ns and recombine with hot holes [100]. So, promoting charge separation should be an effective strategy in enhancing the efficiency of MSC materials. Shiraishi *et al.* reported that Au NPs loaded onto a mixture of anatase/rutile TiO_2 particles promoted efficient aerobic oxidation under visible light [101]. Further study indicates that smooth electron transfer in the Au/rutile/anatase contact site promotes charge-carrier separation in Au, and ultimately enhances the aerobic oxidation of alcohols at ambient temperatures. The 'superstructure' concept was also introduced in suppressing charge recombination [102]. It was proposed that electrons injected from the Au NPs to TiO_2 directionally migrate from the basal surfaces to the edges of the plate-like mesocrystals through the TiO_2 nanocrystal networks. Then, the electrons were temporally stored there for further reactions, which was different from the conventional nanoparticle system (Fig. 9a and 9b). This anisotropic electron flow significantly restrained the charge recombination of these electrons with the holes in the Au NPs and enhanced visible-light photocatalytic activity. In one of our early studies, a multicomponent junction nanostructure (Au–$SrTiO_3$–TiO_2) was constructed for improved visible-light photocatalytic performance in both IPA degradation and water oxidation induced by Au NPs [103]. The schematic illustration of the electron transfer in Au–$SrTiO_3$–TiO_2 composite is shown in Fig. 9c. When Au NPs were irradiated under visible light, the photo-generated electrons from Au NPs were likely to transfer through the $SrTiO_3$–TiO_2 junctions. The whole process was driven by the potential difference caused by the different band levels. As a result, the photo-generated charge carriers in Au NPs can be spatially separated. Thus, charge recombination and backward charge transfer from the

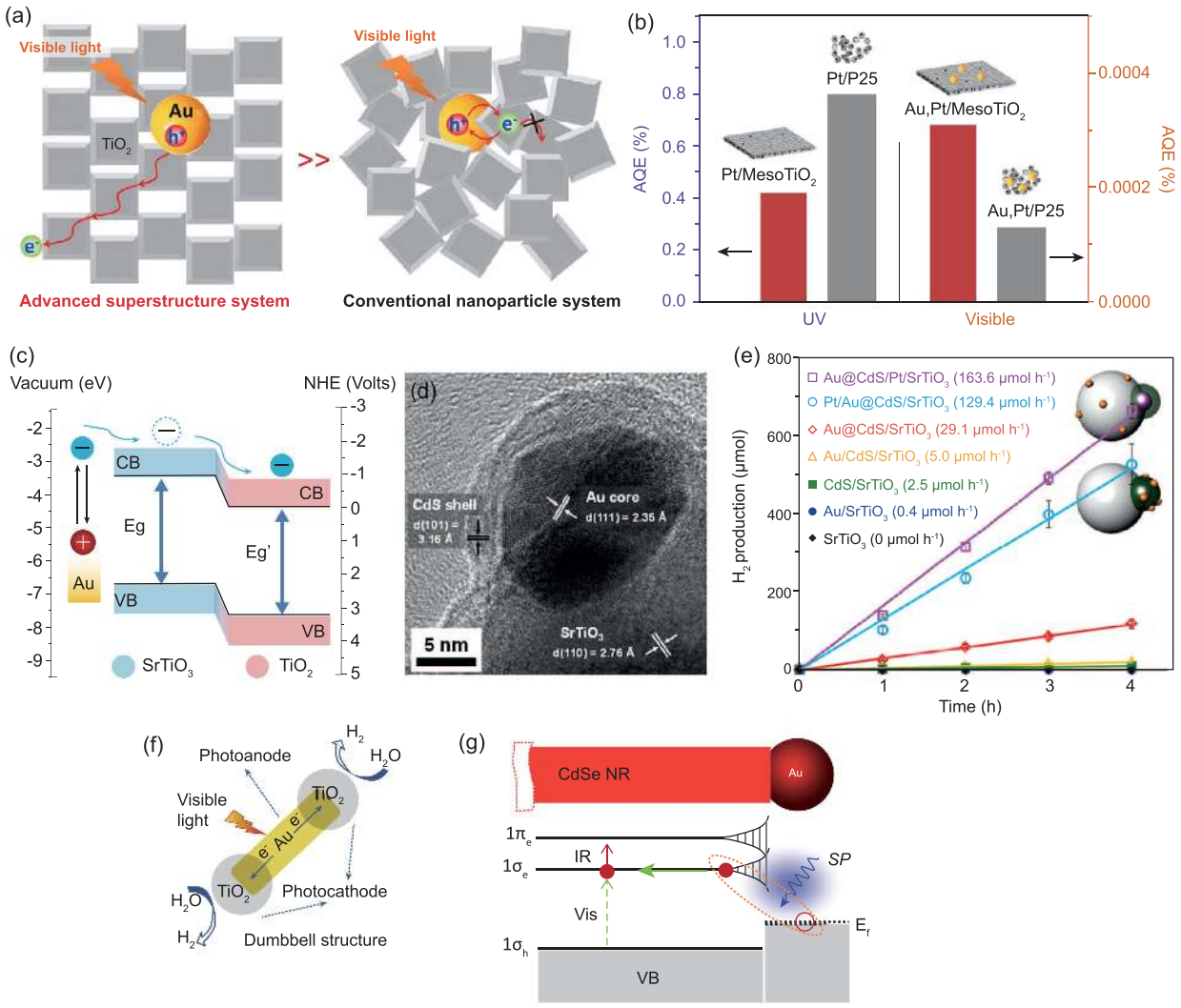

Figure 9. (a) Schematic illustration of electron transfer in advanced superstructure and conventional nanoparticle system. (b) Comparison of hydrogen production performance under UV and visible-light irradiation. Meso TiO_2 refers to mesocrystals TiO_2 [102]. Reprinted with permission from Ref. [102]. Copyright 2014, by the American Chemical Society. (c) Schematic illustration of charge transfer across the Au–$SrTiO_3$–TiO_2 composite [103]. Adapted with permission. Copyright 2015, by The Royal Society of Chemistry. (d) HRTEM image of the interface region of $SrTiO_3$ and Au@CdS. (e) Photocatalytic H_2 production as a function of time under visible-light irradiation ($\lambda > 400$ nm) [104]. Reprinted with permission from Ref. [104]. Copyright 2014, by WILEY-VCH, Weinheim. (f) Structure and mechanism of operation under visible light of an individual Au NR/TiO_2 dumbbell [105]. Reprinted with permission from Ref. [105]. Copyright 2016, by the American Chemical Society. (g) Schematic electronic structure of a CdSe-Au NR [36]. Adapted with permission. Copyright 2015, by American Association for the Advancement of Science.

semiconductor to Au NPs are inhibited. A strategy by introducing another semiconductor was reported by Yi *et al.* [104]. They designed a Au@CdS/$SrTiO_3$ nanostructure, in which $SrTiO_3$ and Au@CdS served as high-performance electron filter and plasmonic photosensitizer, respectively (Fig. 9d and 9e). Further study demonstrated that the ultrafast decay of hot electrons across Au NPs could be significantly reduced by strong coupling with CdS QDs and by a Schottky junction with $SrTiO_3$. Similarly, Wu *et al.* reported an anisotropic growth of TiO_2 onto Au NRs for plasmon-enhanced H_2 evolution [105]. In their experiment, the as-prepared TiO_2-tipped Au NRs have a dumbbell and spatial separation structure. The structure and mechanism of an individual Au NR/TiO_2 dumbbell operated under visible light are shown in Fig. 9f. TiO_2, as a Schottky junction, is claimed to filter out LSPR hot electrons from the Au NRs. Furthermore, with partial exposure in the nanodumbbell structure, Au NRs generated a concentrated electromagnetic field around the semiconductor, and thus hot-electron generation and photocatalytic activity were enhanced.

Interface designing is another strategy applicable to enhancing the efficiency of MSC systems.

It was found that synchronization of charge-carrier separation could be achieved by tailoring the interface of Si–Au–TiO_2 heterostructures via click chemistry [106]. Gold sandwiched between Si and TiO_2 absorbs visible light and transfers hot electrons to nearby semiconductors, which is conducive to progressive photo-conversion efficiency. The authors claimed that appropriate band-edge alignment in composite materials promoted electron–hole separation and ultimately enhanced efficiency. K. Wu *et al.* proposed a pathway from a novel perspective, which was called plasmon-induced interfacial charge-transfer transition (PICTT) (Fig. 9g) [107]. It enables the decay of a plasmon by directly exciting electrons from the metal to a strongly coupled acceptor. They demonstrated this concept in colloidal quantum-confined CdSe-Au NRs heterostructures, in which gold plasmon was intensively damped by CdSe through interfacial electron transfer as shown in Fig. 9g. In this way, high quantum efficiency (>24%) of the PICTT process was achieved. As can be seen from the above cases, proper nanostructure design and interface engineering are of great importance in promoting the efficiency of MSC photocatalysts.

Decoration with cocatalyst

Cocatalyst plays an important role in photocatalysis due to its enhancement in charge-carrier separation and offering active sites for surface reactions. This strategy was also applicable in MIP systems. For instance, Pt/Au/WO_3 photocatalyst utilizing two types of absorption was prepared (Fig. 10a) [108]. Au NPs were first loaded onto WO_3 by colloid photo-deposition, and then Pt NPs as cocatalyst were loaded onto Au particles via photo-deposition. During the water-splitting progress, electrons transferred from Au into the Pt NPs, where H^+ reduction to H_2 occurred. Concerning the electron transfer from Au to semiconductors, it was found that hot-electron transfer would be more efficient, and the resulting photocatalytic activity could be greatly enhanced when TiO_2 was simultaneously excited (together with plasmon excitation of Au) [109]. Mid-gap defect states in semiconductors were also reported to play an important role in the energy transfer from the Ag NPs to AgCl [110]. These findings offer a good perspective for understanding the synergistic effect of Au and semiconductors in designing efficient MSC systems under the full spectrum. Majima *et al.* developed a Pd-modified Au NRs composite material which worked as a light absorber and catalytically active site simultaneously (Fig. 10b) [95]. They synthesized anisotropic Pd-tipped and Pd-covered Au NRs, respectively, by a two-step seed-mediated growth method. The unique bimetallic NRs could exhibit efficient plasmon-enhanced catalytic formic acid dehydrogenation even under 5°C. Apart from H_2-evolution cocatalysts, O_2-evolution cocatalyst-decorated plasmonic NPs, namely Au/IrO_X upon a nanowire-array TiO_2 electrode, were also reported [111]. Their results suggest that the lifetime of plasmon-induced charge carriers could be dramatically improved and the kinetics of chemical reactions further facilitated. A more elaborate nanostructure was developed by Moskovits *et al.* [112]. Crystalline TiO_2 layers, Pt and cobalt-based catalysts, serving as electron filters, H_2-evolution and O_2-evolution cocatalyst, respectively, were decorated onto a uniform array of aligned Au NRs for a plasmonic solar-water splitter, as shown in Fig. 10c and 10d. Moreover, the claimed stability when illuminated with visible light was exceptionally high, even compared with devices based on narrow-band-gap semiconductors. For more information about cocatalyst, readers can refer to reviews that are focused on this subject [92,113]. It can be seen that decoration of MSC materials with cocatalyst is a promising approach for enhancing MIP efficiencies. However, it should be pointed out that this process is more difficult than decorating semiconductors. From one aspect, the presentation of the semiconductor and the small size of the plasmonic metal used in the MIP system require precise preparation control to decorate the cocatalyst to the desired site. From another aspect, the relatively high work function of the plasmonic metal or the metal property of itself may decrease the cocatalyst effect. So work, not only from the preparation method, but also from the decoration strategy are needed.

Particle-size effect of metal

For MIP systems, the property of metal NPs generally plays a crucial role in photocatalytic performance. Particle size is one of these key factors. More and more attention has been paid to its effect in visible-light photocatalysis induced by metals, though consensus has not been reached yet. In this part, related works will be reviewed, and corresponding comments will also be put forward.

It is not strange that plasmonic photocatalytic activity can be enhanced when LSPR absorption is strengthened. Two kinds of Au/TiO_2 catalysts with different particle sizes were prepared by single-step (SS-Au/TiO_2) and multi-step (MS-Au/TiO_2) photo-deposition methods, while Au loadings were kept the same [114]. Accompanied by multi-step photo-deposition, Au particle size increased gradually and MS-Au/TiO_2 (1.0% Au with average

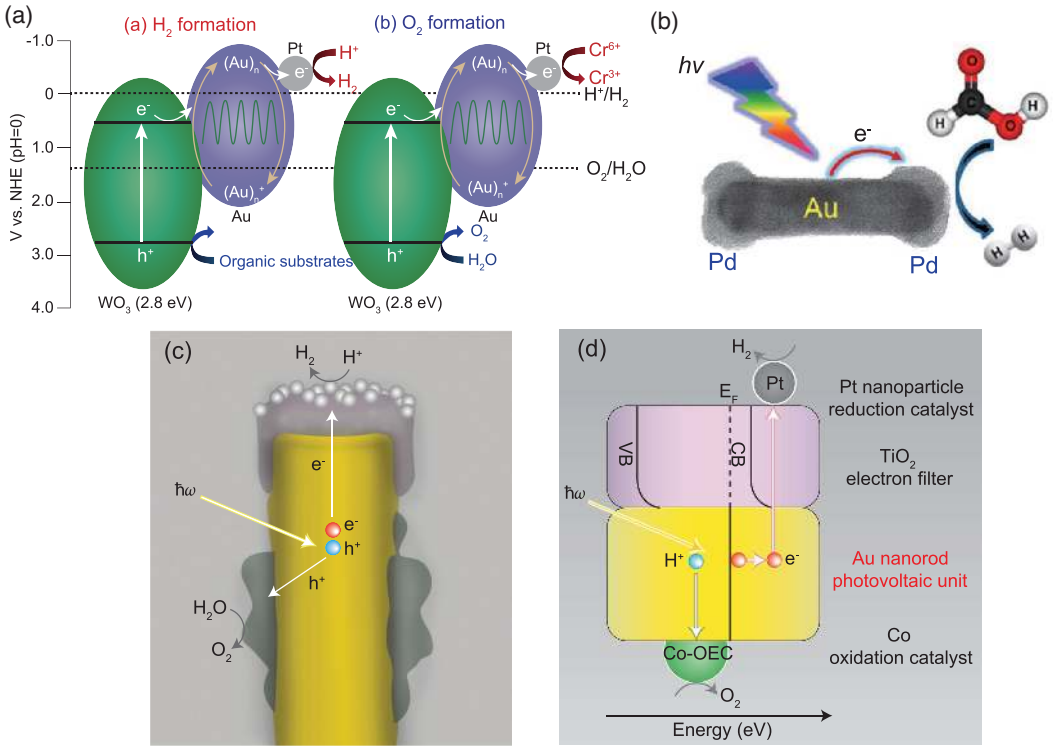

Figure 10. (a) Proposed reaction mechanism for production of H_2 and O_2 in aqueous suspensions of Pt/Au/WO_3 [108]. Reprinted with permission from Ref. [108]. Copyright 2013, by the American Chemical Society. (b) Nanostructure of Pd-decorated Au NR [95]. Reprinted with permission from Ref. [95]. Copyright 2015, by the American Chemical Society. (c) Schematic of the cross-section of an individual photosynthetic unit showing Au NR, TiO_2 cap decorated with Pt NPs which functions as the hydrogen evolution catalyst, and Co-OEC material deposited on the lower portion of gold NR. (d) Energy-level diagram of a plasmonic solar-water splitter over an individual unit, showing the proposed processes occurring in its various parts and in energy space. CB, conduction band; VB, valence band; E_F, Fermi energy [112]. Adapted with permission. Copyright 2013, by Nature Publishing Group.

diameter of 13 nm) exhibited much stronger LSPR absorption than that of SS-Au/TiO_2 (1.0% Au with average diameter of 1.2 nm). In visible-light photocatalytic H_2 evolution, MS-Au/TiO_2 exhibited a much higher H_2-formation rate which was ∼20 times larger than that of SS-Au/TiO_2. This trend seems to be more obvious for larger Au NPs. Wei *et al.* adopted two different methods to prepare Au-TiO_2 heterostructures with 4.4 ± 1.7 nm and 67±17 nm Au NPs, respectively [91]. It is impressive that, in contrast to large Au-P25, no H_2 production was detected for small Au-P25 under $\lambda > 435$ nm irradiation (Fig. 11a). They proposed that energy levels reached by the transferred electrons in TiO_2 CB were determined by electron-transfer efficiencies, while efficient accumulation allowed the transferred electrons to achieve higher energy levels. According to this theory, for small Au-P25, the weaker LSPR intensity of 4.4 nm Au NPs leads to low electron transfer efficiency, and the transferred electrons are insufficient to bring them to an energy level higher than H_2-evolution potential (Fig. 11b). A similar Au size effect was observed by other groups [115–118].

However, opposite phenomena were also reported in the literature. For instance, Au NPs of different sizes (2.9–11.9 nm) were loaded onto a TiO_2 nanocrystalline film over fluorine-doped tin oxide (FTO), and the Au-loading amount was kept constant [119]. It was found that the rate of water oxidation by the PEC cell using Au/TiO_2/FTO anode increased with decreasing mean Au particle size (Fig. 11c). The authors proposed that the density of states (DOS) of Au NPs would decrease along with reducing the particle diameter, which raised an entropic driving force for the forward electron transfer from Au NP to TiO_2 and simultaneously suppressed back electron transfer. In other words, the enhancement was due to the charge separation, as illustrated in Fig. 11d. Philipp Reineck *et al.* also demonstrated that the quantum efficiency had a relationship with the gold nanoparticle size [89]. In their results, Au NPs with a diameter of 5 nm showed a maximum absorbed photon-to-electron

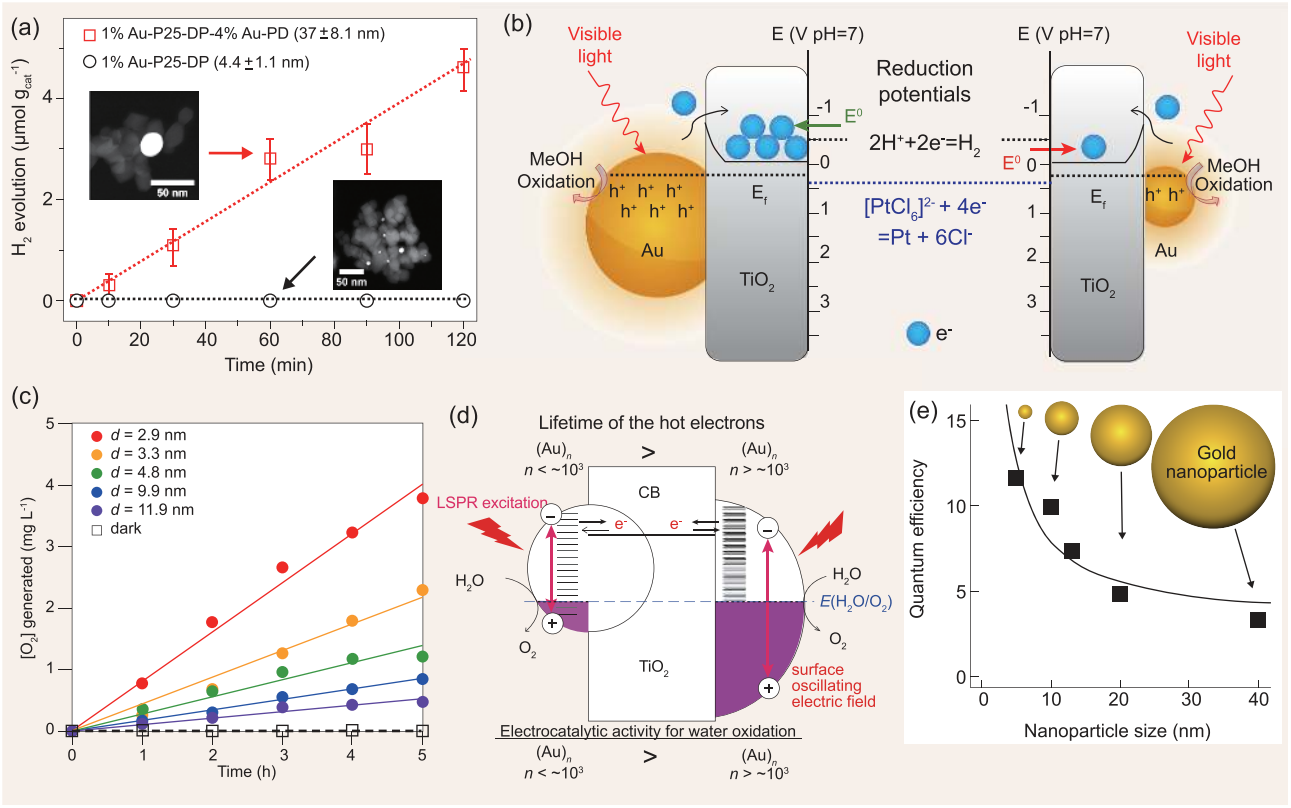

Figure 11. (a) H_2O reduction activities over 1% Au-P25-DP and 1% Au-P25-DP—4% Au-PD photocatalysts under $\lambda > 435$ nm irradiation. (b) Proposed mechanism for manipulating LSPR-mediated electron transfer for photocatalysis by controlling Au NP size [91]. Reprinted with permission from Ref. [91]. Copyright 2014, by the American Chemical Society. (c) Time courses for the rate of O_2 generation. Photocurrent action spectra for Au ($d = 3.3$ and 9.9 nm)/TiO_2/FTO electrodes; the solid curves are absorption spectra. (d) Schematic representation of the Au particle size effect on the activity for water oxidation; the number of the Au atoms in NP (n) with $d = 3.3$, 4.8 and 9.9 nm are estimated to be 5.6×10^2, 1.7×10^3 and 1.5×10^4, respectively, by assuming the hemispherical shape for Au NPs [119]. Reprinted with permission from Ref. [119]. Copyright 2016, by WILEY-VCH, Weinheim. (e) Average maximum APCE values as a function of the Au NP diameter, d. The solid line shows the d^{-1} fit to the experimental data [89]. Reprinted with permission from Ref. [89]. Copyright 2016, by the American Chemical Society.

conversion efficiency (APCE) of 13.3%, while the average APCE declined to 3.3% for the largest Au NPs (40 nm) (Fig. 11e). To enhance PEC water splitting, Kim and Huber *et al.* prepared size-controllable Au nanodot arrays (50, 63 and 83 nm) on indium tin oxide (ITO) substrate with a narrow size distribution (5%) by a direct-contact printing method [120]. Plasmonic enhancement was observed over all nanostructures with Au nanodots; however, the measured enhancement for light on/off experiments was 25 times higher for 50-nm Au size and 10 times for 83-nm Au nanodots. These activities were proportional to a defined quality factor, i.e. LSPR peak energy divided by LSPR line width. They claimed that the enhanced PEC performance with decreasing Au nanodot size was probably caused by more charge carriers photo-generated at the Au/TiO_2 interface induced by local field enhancement. Analogous observation was also reported by Tatsuma's group in a diad system with Au clusters and Au NPs [121]. In addition to these two opposite conclusions on Au particle size, there are other findings that an optimized size exists. In a study of photocatalytic CO_2 conversion over Pt/TiO_2, the incorporation of Au NPs (with sizes of 4, 8, 18 and 26 nm) was found to enhance catalytic activity, while the optimum sizes of Au NPs were determined to be 18 nm [122].

For practical catalyst systems, the distribution of particle size is usually a volcano type. That is, both large and small metal NPs exist, though the proportion is different. One may suspect that the conclusion is reliable when particle distribution is not narrow enough to exclude interference of undesired particles. On the other hand, the role played by metal NPs with different sizes in MIP is also an interesting subject. The subsequent studies paid much attention to this issue. One experiment from Li *et al.* achieved synergetic promotion of Au NPs with different sizes in visible-light photocatalytic H_2 evolution over Au/TiO_2 [123]. It is proposed that electrons of large Au NPs were excited by visible light

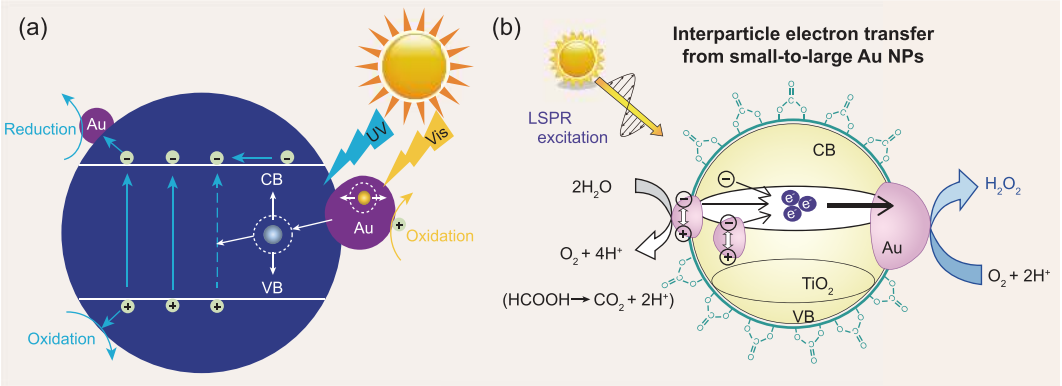

Figure 12. (a) Promotion effects of Au particles on the photocatalytic activity of TiO_2 under UV-visible-light irradiation [123]. Adapted with permission. Copyright 2013, by The Royal Society of Chemistry. (b) A mechanism proposed for the BM-Au/TiO_2-CO_3^{2-} plasmonic photocatalysed reduction of O_2 to H_2O_2 [124]. Reprinted with permission from Ref. [124]. Copyright 2016, by WILEY-VCH, Weinheim.

through LSPR and subsequently transferred to the CB of adjacent TiO_2, while small Au NPs on TiO_2 could act as efficient cocatalysts and trap photoexcited electrons from the CB of TiO_2 (Fig. 12a). However, other similar research proposed an opposite mechanism. Au NP-loaded TiO_2 with a bimodal size distribution around 10.6 nm and 2.3 nm (BM-Au/TiO_2) was prepared by Tada's group [124]. An efficient visible-light-driven reduction of O_2 to H_2O_2 in pure water was observed. They claimed that visible-light irradiation of BM-Au/TiO_2 gave rise to interfacial electron transfer from small to large Au NPs through the CB of TiO_2, as shown in Fig. 12b. The oxidizing and reducing abilities were induced on small and large Au NPs, respectively.

As can be seen from the above studies, the size of metal largely influences the catalytic activity of MIP systems under visible-light irradiation. However, no satisfactory conclusion on this issue has been arrived at at this stage, though much work has been carried out. The complexity of these conclusions indicates that the particle size of metal is more complicated than expected for MIP systems. To address this issue, much attention should be paid to clarifying the different roles played by metal NPs in MIP systems, e.g. Au particles act mainly for cocatalyst or light-harvesting (field enhancement) or hot-electron reaction. Distinguishing these situations is helpful to understanding the size effect of metal and designing efficient MSC photocatalysts. On the other hand, in-depth study is needed for better understanding the physical mechanism related to the size effect. Fortunately, related work has been carried out. For example, Tada's group studied the size dependence of the Fermi energy of gold nanoparticles [125]. TiO_2-supported Au NPs with varying sizes were prepared by the deposition-precipitation method. The Fermi energy of Au NPs directly coupled with TiO_2 at the photostationary state (E_F') has been determined by using S/S^{2-} as a redox probe. It was found that the E_F' value went up as the mean size of the Au NPs increased, which led to enhanced efficiency of the interfacial electron transfer between TiO_2 and Au NPs. A symmetrical study on Au/TO_2 was also carried out [126]. They compared the photocatalytic activity between Au/anatase and Au/rutile under both UV- and visible-light irradiation. It was found that Au particle size for the Au/rutile system showed a volcano-shaped curve, with a maximum diameter of about 5 nm, while the activity of the Au/anatase system weakly depended on the Au diameter. Moreover, Au NP loading on rutile caused significant decoupling between the LSPR and interband transition mode, which elongated the LSPR lifetime. It is claimed that the optimum diameter value was determined by the factors of the LSPR absorption intensity, interfacial electron-transfer efficiency and even the surface area.

OUTLOOK AND PROSPECTIVES

Exploring light absorption of metal NPs in photocatalysis represents a class of novel and promising approaches in exploring efficient visible-light-responsive photocatalysts. However, to achieve this goal, there are still many challenges to be addressed in exploring efficient MIP to its full potential.

Deeper understanding the mechanism behind MIP is urgently needed. It is undoubted that clear understanding of the mechanism is crucial in designing efficient MSC photocatalysts. The photosensitization and enhancement mechanisms of metal in MIP include, but are not limited to, the aspects stated above; however, consensus is far from being reached on this issue [31,36]. Compared with various findings in plasmonic enhancement, work

focused on the mechanism is limited. Moreover, in-situ characterization and precise nanostructure design are preferred, as they generally offer deep insight in addition to electromagnetic simulation [15,24,27]. One of the representative issues concerning the mechanism is the principle of the match between metal and semiconductor. The wide use of TiO_2 in metal photosensitization cannot be simply ascribed to its stability and nontoxicity. So far, the Au photosensitization effect is most prominent over TiO_2 or $SrTiO_3$, while this effect is very limited when it is composited with other semiconductors with large band-gaps, such as ZnO and $NaNbO_3$. However, the physical mechanism of match or mismatch in MIP systems is rarely touched upon. Another issue under debate is the driving force in MIP. Take Au, for example; the absorption of Au NPs in the visible-light region comprises two models, i.e. LSPR and interband transitions. The observed photosensitization or enhancement effect is generally ascribed to LSPR at an early stage. Nevertheless, more and more experimental results indicate that interband transitions are also involved, or even the main driving force, in MIP systems [20,21,23,24,119,124]. From this perspective, AQE experiments are suggested to be offered in MIP evaluations.

The second future research aspect is to improve the efficiency of MIP, in particular metal photosensitization for harsh photocatalytic reactions like water splitting and CO_2 photoreduction. Until now, the efficiency of photocatalytic water splitting using MSC materials is relatively low and far behind the theoretically predicted efficiency. Most of the research mainly focused on developing different systems in this field, while it is still at a preliminary stage in pursuing efficient MIP systems. It is highly important to devote more effort towards accelerating the H_2- or O_2-evolution rate based on underlying mechanism understanding. The situation is similar in PEC and photovoltaics. To address this issue, various strategies developed in the literature for enhancing MIP efficiencies have been summarized in this review. As stated above, much attention should be paid to the leaving holes on metal, as its oxidation ability may restrict the overall efficiency, while hot electrons transfer from metal to CB of semiconductors where proton is reduced to H_2. Another important factor that should be taken into account is decreasing the use of Au. Most of the prepared plasmonic photocatalysts are based on Au nanostructures; however, the cost of composite materials has to be reduced, as Au is very expensive. Ag-based plasmonic composites have been demonstrated to be rather effective in the degradation of organic pollutions, and various nanostructures have been developed [127–131]. However, the easy oxidation property of Ag should be considered in designing MSCs [128,131,132]. Much effort is highly needed in developing efficient MIP systems based on Ag or Cu.

Thirdly, rational design and precise control of plasmonic metal in MSC materials are highly needed. This is of great importance not only for understanding the mechanism of MIP, but also for developing efficient composite photocatalysts. General preparation methods without good control result in complexity of the MSC system, which makes it difficult to study target factors in MIP [133,134]. For example, the coexistence of both large and small particles or wide particle distribution leads to difficulty in studying the particle-size effect in MIP. Novel synthetic methods such as atomic layer deposition (ALD) are interesting aspects to explore. Precise arrangement control of plasmonic metals is of importance in modulating the strength of the electromagnetic field induced by LSPR and ultimately influences plasmonic enhancement [135]. Moreover, design strategies are also crucial to the development of plasmonic–photovoltaic systems with enhanced efficiency. That is, more research effort is required in achieving a better control of the size, shape and nanostructure of each component, as well as the junction interface in MSC materials [136].

Recent research progress on exploring MIP systems suggests that the integration of metal NPs with semiconductors is a promising strategy in developing efficient visible-light-responsive materials. The exploration of the above-mentioned challenges will lead to rapid progress in this field. It is reasonable to believe that such efforts will enable obvious breakthroughs in MIP field, making it an important strategy in visible-light photocatalysis and solar-energy conversion.

FUNDING

This work was supported by the National Basic Research Program of China (2014CB239301) and the National Natural Science Foundation of China (21673157 and 21503145).

REFERENCES

1. Chen H, Shao L and Li Q *et al.* Gold nanorods and their plasmonic properties. *Chem Soc Rev* 2013; **42**: 2679–724.
2. Zhao G, Kozuka H and Yoko T. Sol-gel preparation and photoelectrochemical properties of TiO_2 films containing Au and Ag metal particles. *Thin Solid Films* 1996; **277**: 147–54.
3. Link S and El-Sayed MA. Size and temperature dependence of the plasmon absorption of colloidal gold nanoparticles. *J Phys Chem B* 1999; **103**: 4212–7.

4. Atwater HA and Polman A. Plasmonics for improved photovoltaic devices. *Nat Mater* 2010; **9**: 205–13.
5. Kelly KL, Coronado E and Zhao LL *et al.* The optical properties of metal nanoparticles: the influence of size, shape, and dielectric environment. *J Phys Chem B* 2002; **107**: 668–77.
6. Naik GV, Shalaev VM and Boltasseva A. Alternative plasmonic materials: beyond gold and silver. *Adv Mater* 2013; **25**: 3264–94.
7. Creighton JA and Eadon DG. Ultraviolet-visible absorption spectra of the colloidal metallic elements. *J Chem Soc Faraday Trans* 1991; **87**: 3881.
8. Xia Y, Xiong Y and Lim B *et al.* Shape-controlled synthesis of metal nanocrystals: simple chemistry meets complex physics? *Angew Chem Int Ed* 2009; **48**: 60–103.
9. Langhammer C, Yuan Z and Zorić I *et al.* Plasmonic properties of supported Pt and Pd nanostructures. *Nano Lett* 2006; **6**: 833–8.
10. Sonnichsen C, Franzl T and Wilk T *et al.* Drastic reduction of plasmon damping in gold nanorods. *Phys Rev Lett* 2002; **88**: 077402.
11. Halas NJ, Lal S and Chang WS *et al.* Plasmons in strongly coupled metallic nanostructures. *Chem Rev* 2011; **111**: 3913–61.
12. Tian Y and Tatsuma T. Plasmon-induced photoelectrochemistry at metal nanoparticles supported on nanoporous TiO_2. *Chem Commun* 2004; 1810–1.
13. Tian Y and Tatsuma T. Mechanisms and applications of plasmon-induced charge separation at TiO_2 films loaded with gold nanoparticles. *J Am Chem Soc* 2005; **127**: 7632–7.
14. Furube A, Du L and Hara K *et al.* Ultrafast plasmon-induced electron transfer from gold nanodots into TiO_2 nanoparticles. *J Am Chem Soc* 2007; **129**: 14852–3.
15. Kazuma E and Tatsuma T. In situ nanoimaging of photoinduced charge separation at the plasmonic au nanoparticle-TiO_2 interface. *Adv Mater Interfaces* 2014; **1**: 1400066.
16. Xu D, Liu D and Xie T *et al.* Plasmon resonance scattering at perovskite $CH_3NH_3PbI_3$ coated single gold nanoparticles: evidence for electron transfer. *Chem Commun* 2016; **52**: 9933–6.
17. Knight MW, Sobhani H and Nordlander P *et al.* Photodetection with active optical antennas. *Science* 2011; **332**: 702–4.
18. Hou W and Cronin SB. A review of surface plasmon resonance-enhanced photocatalysis. *Adv Funct Mater* 2013; **23**: 1612–9.
19. Govorov AO, Zhang H and Gun'ko YK. Theory of photoinjection of hot plasmonic carriers from metal nanostructures into semiconductors and surface molecules. *J Phys Chem C* 2013; **117**: 16616–31.
20. Liu L, Li P and Adisak B *et al.* Gold photosensitized $SrTiO_3$ for visible-light water oxidation induced by Au interband transitions. *J Mater Chem A* 2014; **2**: 9875–82.
21. Liu M, Zhou W and Wang T *et al.* High performance Au-Cu alloy for enhanced visible-light water splitting driven by coinage metals. *Chem Commun* 2016; **52**: 4694–7.
22. Shiraishi Y, Sakamoto H and Sugano Y *et al.* Pt-Cu bimetallic alloy nanoparticles supported on anatase TiO_2: highly active catalysts for aerobic oxidation driven by visible light. *ACS Nano* 2013; **7**: 9287–97.
23. Sarina S, Zhu H-Y and Xiao Q *et al.* Viable photocatalysts under solar-spectrum irradiation: nonplasmonic metal nanoparticles. *Angew Chem Int Ed* 2014; **53**: 2935–40.
24. Priebe JB, Karnahl M and Junge H *et al.* Water reduction with visible light: synergy between optical transitions and electron transfer in Au-TiO_2 catalysts visualized by in situ EPR spectroscopy. *Angew Chem Int Ed* 2013; **52**: 11420–4.
25. Babicheva VE, Zhukovsky SV and Ikhsanov RS *et al.* Hot electron photoemission from plasmonic nanostructures: the role of surface photoemission and transition absorption. *ACS Photonics* 2015; **2**: 1039–48.
26. Anger P, Bharadwaj P and Novotny L. Enhancement and quenching of single-molecule fluorescence. *Phys Rev Lett* 2006; **96**: 113002.
27. Torimoto T, Horibe H and Kameyama T *et al.* Plasmon-enhanced photocatalytic activity of cadmium sulfide nanoparticle immobilized on silica-coated gold particles. *J Phys Chem Lett* 2011; **2**: 2057–62.
28. Standridge SD, Schatz GC and Hupp JT. Distance dependence of plasmon-enhanced photocurrent in dye-sensitized solar cells. *J Am Chem Soc* 2009; **131**: 8407–9.
29. Kumar MK, Krishnamoorthy S and Tan LK *et al.* Field effects in plasmonic photocatalyst by precise SiO_2 thickness control using atomic layer deposition. *ACS Catal* 2011; **1**: 300–8.
30. Thomann I, Pinaud BA and Chen ZB *et al.* Plasmon enhanced solar-to-fuel energy conversion. *Nano Lett* 2011; **11**: 3440–6.
31. Cushing SK, Li J and Meng F *et al.* Photocatalytic activity enhanced by plasmonic resonant energy transfer from metal to semiconductor. *J Am Chem Soc* 2012; **134**: 15033–41.
32. Cushing SK and Wu N. Progress and perspectives of plasmon-enhanced solar energy conversion. *J Phys Chem Lett* 2016; **7**: 666–75.
33. Li J, Cushing SK and Bright J *et al.* Ag@Cu_2O core-shell nanoparticles as visible-light plasmonic photocatalysts. *ACS Catal* 2013; **3**: 47–51.
34. Li J, Cushing SK and Meng F *et al.* Plasmon-induced resonance energy transfer for solar energy conversion. *Nat Photonics* 2015; **9**: 601–7.
35. Cushing SK, Li J and Bright J *et al.* Controlling plasmon-induced resonance energy transfer and hot electron injection processes in metal@TiO_2 core-shell nanoparticles. *J Phys Chem C* 2015; **119**: 16239–44.
36. Wu K, Chen J and McBride JR *et al.* Efficient hot-electron transfer by a plasmon-induced interfacial charge-transfer transition. *Science* 2015; **349**: 632–5.
37. Li J, Cushing SK and Zheng P *et al.* Plasmon-induced photonic and energy-transfer enhancement of solar water splitting by a hematite nanorod array. *Nat Commun* 2013; **4**: 2651.
38. Liu H, Meng X and Thang Duy D *et al.* Conversion of carbon dioxide by methane reforming under visible-light irradiation: surface-plasmon-mediated nonpolar molecule activation. *Angew Chem Int Ed* 2015; **54**: 11545–9.
39. Zhang H, Wang T and Wang J *et al.* Surface-plasmon-enhanced photodriven CO_2 reduction catalyzed by metal-organic-framework-derived iron nanoparticles encapsulated by ultrathin carbon layers. *Adv Mater* 2016; **28**: 3703–10.
40. Meng X, Wang T and Liu L *et al.* Photothermal conversion of CO_2 into CH_4 with H_2 over Group VIII nanocatalysts: an alternative approach for solar fuel production. *Angew Chem Int Ed* 2014; **53**: 11478–82.
41. Zhou X, Liu G and Yu J *et al.* Surface plasmon resonance-mediated photocatalysis by noble metal-based composites under visible light. *J Mater Chem* 2012; **22**: 21337.
42. Kale MJ, Avanesian T and Christopher P. Direct photocatalysis by plasmonic nanostructures. *ACS Catal* 2013; **4**: 116–28.
43. Linic S, Christopher P and Xin H *et al.* Catalytic and photocatalytic transformations on metal nanoparticles with targeted geometric and plasmonic properties. *Acc Chem Res* 2013; **46**: 1890–9.
44. Xiao M, Jiang R and Wang F *et al.* Plasmon-enhanced chemical reactions. *J Mater Chem A* 2013; **1**: 5790.
45. Lou Z, Wang Z and Huang B *et al.* Synthesis and activity of plasmonic photocatalysts. *Chem Cat Chem* 2014; **6**: 2456–76.

46. Xiao Q, Jaatinen E and Zhu H. Direct photocatalysis for organic synthesis by using plasmonic-metal nanoparticles irradiated with visible light. *Chem–Asian J* 2014; **9**: 3046–64.
47. Long R, Li Y and Song L *et al.* Coupling solar energy into reactions: materials design for surface plasmon-mediated catalysis. *Small* 2015; **11**: 3873–89.
48. Fujishima A and Honda K. Electrochemical photolysis of water at a semiconductor electrode. *Nature* 1972; **238**: 37–8.
49. Silva CG, Juarez R and Marino T *et al.* Influence of excitation wavelength (UV or visible light) on the photocatalytic activity of titania containing gold nanoparticles for the generation of hydrogen or oxygen from water. *J Am Chem Soc* 2011; **133**: 595–602.
50. Primo A, Marino T and Corma A *et al.* Efficient visible-light photocatalytic water splitting by minute amounts of gold supported on nanoparticulate CeO_2 obtained by a biopolymer templating method. *J Am Chem Soc* 2011; **133**: 6930–3.
51. Chen HM, Chen CK and Chen C-J *et al.* Plasmon inducing effects for enhanced photoelectrochemical water splitting: x-ray absorption approach to electronic structures. *ACS Nano* 2012; **6**: 7362–72.
52. Seh ZW, Liu S and Low M *et al.* Janus Au-TiO_2 photocatalysts with strong localization of plasmonic near-fields for efficient visible-light hydrogen generation. *Adv Mater* 2012; **24**: 2310–4.
53. Zheng Z, Tachikawa T and Majima T. Single-particle study of Pt-modified Au nanorods for plasmon-enhanced hydrogen generation in visible to near-infrared region. *J Am Chem Soc* 2014; **136**: 6870–3.
54. Mubeen S, Lee J and Singh N *et al.* An autonomous photosynthetic device in which all charge carriers derive from surface plasmons. *Nat Nanotechnol* 2013; **8**: 247–51.
55. Chandrasekharan N and Kamat PV. Improving the photoelectrochemical performance of nanostructured TiO_2 films by adsorption of gold nanoparticles. *J Phys Chem B* 2000; **104**: 10851–7.
56. Liu ZW, Hou WB and Pavaskar P *et al.* Plasmon resonant enhancement of photocatalytic water splitting under visible illumination. *Nano Lett* 2011; **11**: 1111–6.
57. Li J, Cushing SK and Zheng P *et al.* Solar hydrogen generation by a CdS-Au-TiO_2 sandwich nanorod array enhanced with Au nanoparticle as electron relay and plasmonic photosensitizer. *J Am Chem Soc* 2014; **136**: 8438–49.
58. DuChene JS, Sweeny BC and Johnston-Peck AC *et al.* Prolonged hot electron dynamics in plasmonic-metal/semiconductor heterostructures with implications for solar photocatalysis. *Angew Chem Int Ed* 2014; **53**: 7887–91.
59. Bai S, Li X and Kong Q *et al.* Toward enhanced photocatalytic oxygen evolution: synergetic utilization of plasmonic effect and Schottky junction via interfacing facet selection. *Adv Mater* 2015; **27**: 3444–52.
60. Halmann M. Photoelectrochemical reduction of aqueous carbon dioxide on p-type gallium phosphide in liquid junction solar cells. *Nature* 1978; **275**: 115–6.
61. Inoue T, Fujishima A and Konishi S *et al.* Photoelectrocatalytic reduction of carbon dioxide in aqueous suspensions of semiconductor powders. *Nature* 1979; **277**: 637–8.
62. Habisreutinger SN, Schmidt-Mende L and Stolarczyk JK. Photocatalytic reduction of CO_2 on TiO_2 and other semiconductors. *Angew Chem Int Ed* 2013; **52**: 7372–408.
63. Tu W, Zhou Y and Zou Z. Photocatalytic conversion of CO_2 into renewable hydrocarbon fuels: state-of-the-art accomplishment, challenges, and prospects. *Adv Mater* 2014; **26**: 4607–26.
64. Ozin GA. Throwing new light on the reduction of CO_2. *Adv Mater* 2015; **27**: 1957–63.
65. Hou WB, Hung WH and Pavaskar P *et al.* Photocatalytic conversion of CO_2 to hydrocarbon fuels via plasmon-enhanced absorption and metallic interband transitions. *ACS Catal* 2011; **1**: 929–36.
66. Zhang Z, Wang Z and Cao S-W *et al.* Au/Pt nanoparticle-decorated TiO_2 nanofibers with plasmon-enhanced photocatalytic activities for solar-to-fuel conversion. *J Phys Chem C* 2013; **117**: 25939–47.
67. Kumar D, Lee A and Lee T *et al.* Ultrafast and efficient transport of hot plasmonic electrons by graphene for Pt free, highly efficient visible-light responsive photocatalyst. *Nano Lett* 2016; **16**: 1760–7.
68. Tu W, Zhou Y and Li H *et al.* Au@TiO_2 yolk–shell hollow spheres for plasmon-induced photocatalytic reduction of CO_2 to solar fuel via a local electromagnetic field. *Nanoscale* 2015; **7**: 14232–6.
69. Mukherjee S, Libisch F and Large N *et al.* Hot electrons do the impossible: plasmon-induced dissociation of H_2 on Au. *Nano Lett* 2013; **13**: 240–7.
70. Liu H, Meng X and Dao TD *et al.* Conversion of carbon dioxide by methane reforming under visible-light irradiation: surface-plasmon-mediated nonpolar molecule activation. *Angew Chem Int Ed* 2015; **54**: 11545–9.
71. Liu H, Li M and Dao TD *et al.* Design of PdAu alloy plasmonic nanoparticles for improved catalytic performance in CO_2 reduction with visible light irradiation. *Nano Energy* 2016; **26**: 398–404.
72. Zhang H, Wang T and Wang J *et al.* Surface-plasmon-enhanced photodriven CO_2 reduction catalyzed by metal–organic-framework-derived iron nanoparticles encapsulated by ultrathin carbon layers. *Adv Mater* 2016; **28**: 3703–10.
73. Meng X, Wang T and Liu L *et al.* Photothermal conversion of CO_2 into CH_4 with H_2 over Group VIII nanocatalysts: an alternative approach for solar fuel production. *Angew Chem Int Ed* 2014; **126**: 11662–6.
74. Schrauzer G and Guth T. Photocatalytic reactions. 1. Photolysis of water and photoreduction of nitrogen on titanium dioxide. *J Am Chem Soc* 1977; **99**: 7189–93.
75. Rusina O, Eremenko A and Frank G *et al.* Nitrogen photofixation at nanostructured iron titanate films. *Angew Chem Int Ed* 2001; **40**: 3993–5.
76. Zhu D, Zhang L and Ruther RE *et al.* Photo-illuminated diamond as a solid-state source of solvated electrons in water for nitrogen reduction. *Nat Mater* 2013; **12**: 836–41.
77. Banerjee A, Yuhas BD and Margulies EA *et al.* Photochemical nitrogen conversion to ammonia in ambient conditions with FeMoS-chalcogels. *J Am Chem Soc* 2015; **137**: 2030–4.
78. Li H, Shang J and Ai Z *et al.* Efficient visible light nitrogen fixation with BiOBr nanosheets of oxygen vacancies on the exposed {001} facets. *J Am Chem Soc* 2015; **137**: 6393–9.
79. Oshikiri T, Ueno K and Misawa H. Plasmon-induced ammonia synthesis through nitrogen photofixation with visible light irradiation. *Angew Chem Int Ed* 2014; **53**: 9802–5.
80. Oshikiri T, Ueno K and Misawa H. Selective dinitrogen conversion to ammonia using water and visible light through plasmon-induced charge separation. *Angew Chem Int Ed* 2016; **55**: 3942–6.
81. Martirez JMP and Carter EA. Thermodynamic constraints in using AuM (M= Fe, Co, Ni, and Mo) alloys as N_2 dissociation catalysts: functionalizing a plasmon-active metal. *ACS nano* 2016; **10**: 2940–9.
82. Ali M, Zhou F and Chen K *et al.* Nanostructured photoelectrochemical solar cell for nitrogen reduction using plasmon-enhanced black silicon. *Nat Commun* 2016; **7**: 11335.
83. Holmen A. Direct conversion of methane to fuels and chemicals. *Catal Today* 2009; **142**: 2–8.
84. Chen X, Li Y and Pan X *et al.* Photocatalytic oxidation of methane over silver decorated zinc oxide nanocatalysts. *Nat Commun* 2016; **7**: 12273.

85. Kudo A and Miseki Y. Heterogeneous photocatalyst materials for water splitting. *Chem Soc Rev* 2009; **38**: 253–78.
86. White TP and Catchpole KR. Plasmon-enhanced internal photoemission for photovoltaics: theoretical efficiency limits. *Appl Phys Lett* 2012; **101**: 073905.
87. Boriskina SV, Zhuo J and Hsu W-C *et al.* Limiting efficiencies of solar energy conversion and photo-detection via internal emission of hot electrons and hot holes in gold. *Infrared Remote Sensing and Instrumentation XXIII* 2015; **9608**: 960816.
88. Cushing SK, Bristow AD and Wu N. Theoretical maximum efficiency of solar energy conversion in plasmonic metal-semiconductor heterojunctions. *Phys Chem Chem Phys* 2015; **17**: 30013–22.
89. Reineck P, Brick D and Mulvaney P *et al.* Plasmonic hot electron solar cells: the effect of nanoparticle size on quantum efficiency. *J Phys Chem Lett* 2016; **7**: 4137–41.
90. Primo A, Corma A and Garcia H. Influence of excitation wavelength (UV or visible light) on the photocatalytic activity of titania containing gold nanoparticles for the generation of hydrogen or oxygen from water. *Phys Chem Chem Phys* 2011; **13**: 886–910.
91. Qian K, Sweeny BC and Johnston-Peck AC *et al.* Surface plasmon-driven water reduction: gold nanoparticle size matters. *J Am Chem Soc* 2014; **136**: 9842–5.
92. Ran J, Zhang J and Yu J *et al.* Earth-abundant cocatalysts for semiconductor-based photocatalytic water splitting. *Chem Soc Rev* 2014; **43**: 7787–812.
93. Link S, Mohamed MB and El-Sayed MA. Simulation of the optical absorption spectra of gold nanorods as a function of their aspect ratio and the effect of the medium dielectric constant. *J Phys Chem B* 1999; **103**: 3073–7.
94. Liu L, Ouyang S and Ye J. Gold-nanorod-photosensitized titanium dioxide with wide-range visible-light harvesting based on localized surface plasmon resonance. *Angew Chem Int Ed* 2013; **52**: 6689–93.
95. Zheng Z, Tachikawa T and Majima T. Plasmon-enhanced formic acid dehydrogenation using anisotropic Pd-Au nanorods studied at the single-particle level. *J Am Chem Soc* 2015; **137**: 948–57.
96. Wang J-H, Chen M and Luo Z-J *et al.* Ceria-coated gold nanorods for plasmon-enhanced near-infrared photocatalytic and photoelectrochemical performances. *J Phys Chem C* 2016; **120**: 14805–12.
97. Liu L, Dao TD and Kodiyath R *et al.* Plasmonic janus-composite photocatalyst comprising Au and C-TiO_2 for enhanced aerobic oxidation over a broad visible-light range. *Adv Funct Mater* 2014; **24**: 7754–62.
98. Kodiyath R, Manikandan M and Liu L *et al.* Visible-light photodecomposition of acetaldehyde by TiO_2-coated gold nanocages: plasmon-mediated hot electron transport via defect states. *Chem Commun* 2014; **50**: 15553–6.
99. Gołąbiewska A, Malankowska A and Jarek M *et al.* The effect of gold shape and size on the properties and visible light-induced photoactivity of Au-TiO_2. *Appl Catal B* 2016; **196**: 27–40.
100. Clavero C. Plasmon-induced hot-electron generation at nanoparticle/metal-oxide interfaces for photovoltaic and photocatalytic devices. *Nat Photonics* 2014; **8**: 95–103.
101. Tsukamoto D, Shiraishi Y and Sugano Y *et al.* Gold nanoparticles located at the interface of anatase/rutile TiO_2 particles as active plasmonic photocatalysts for aerobic oxidation. *J Am Chem Soc* 2012; **134**: 6309–15.
102. Bian Z, Tachikawa T and Zhang P *et al.* Au/TiO_2 superstructure-based plasmonic photocatalysts exhibiting efficient charge separation and unprecedented activity. *J Am Chem Soc* 2014; **136**: 458–65.
103. Liu L, Li P and Wang T *et al.* Constructing a multicomponent junction for improved visible-light photocatalytic performance induced by Au nanoparticles. *Chem Commun* 2015; **51**: 2173–6.
104. Yu S, Kim YH and Lee SY *et al.* Hot-electron-transfer enhancement for the efficient energy conversion of visible light. *Angew Chem Int Ed* 2014; **53**: 11203–7.
105. Wu B, Liu D and Mubeen S *et al.* Anisotropic growth of TiO_2 onto gold nanorods for plasmon-enhanced hydrogen production from water reduction. *J Am Chem Soc* 2016; **138**: 1114–7.
106. Behara DK, Sharma GP and Upadhyay AP *et al.* Synchronization of charge carrier separation by tailoring the interface of Si–Au–TiO_2 heterostructures via click chemistry for PEC water splitting. *Chem Eng Sci* 2016; **154**: 150–69.
107. Wu K, Chen J and McBride JR *et al.* Efficient hot-electron transfer by a plasmon-induced interfacial charge-transfer transition. *Science* 2015 **349:** 632–5.
108. Tanaka A, Hashimoto K and Kominami H. Visible-light-induced hydrogen and oxygen formation over Pt/Au/WO_3 photocatalyst utilizing two types of photoabsorption due to surface plasmon resonance and band-gap excitation. *J Am Chem Soc* 2013; **136**: 586–9.
109. Zhang Z, Li A and Cao SW *et al.* Direct evidence of plasmon enhancement on photocatalytic hydrogen generation over Au/Pt-decorated TiO_2 nanofibers. *Nanoscale* 2014; **6**: 5217–22.
110. Ma X, Dai Y and Yu L *et al.* Electron–hole pair generation of the visible-light plasmonic photocatalyst Ag@AgCl: enhanced optical transitions involving midgap defect states of AgCl. *J Phys Chem C* 2014; **118**: 12133–40.
111. Hung S-F, Xiao F-X and Hsu Y-Y *et al.* Iridium oxide-assisted plasmon-induced hot carriers: improvement on kinetics and thermodynamics of hot carriers. *Adv Energy Mater* 2016; **6**: 1501339.
112. Mubeen S, Lee J and Singh N *et al.* An autonomous photosynthetic device in which all charge carriers derive from surface plasmons. *Nat Nanotechnol* 2013; **8**: 247–51.
113. Meng X, Liu L and Ouyang S *et al.* Nanometals for solar-to-chemical energy conversion: from semiconductor-based photocatalysis to plasmon-mediated photocatalysis and photo-thermocatalysis. *Adv Mater* 2016; **28**: 6781–803.
114. Tanaka A, Sakaguchi S and Hashimoto K *et al.* Preparation of Au/TiO_2 exhibiting strong surface plasmon resonance effective for photoinduced hydrogen formation from organic and inorganic compounds under irradiation of visible light. *Catal Sci Technol* 2012; **2**: 907–9.
115. Zhao WW, Tian CY and Xu JJ *et al.* The coupling of localized surface plasmon resonance-based photoelectrochemistry and nanoparticle size effect: towards novel plasmonic photoelectrochemical biosensing. *Chem Commun* 2012; **48**: 895–7.
116. Yuzawa H, Yoshida T and Yoshida H. Gold nanoparticles on titanium oxide effective for photocatalytic hydrogen formation under visible light. *Appl Catal B* 2012; **115–116**: 294–302.
117. Kowalska E, Rau S and Ohtani B. Plasmonic titania photocatalysts active under UV and visible-light irradiation: Influence of gold amount, size, and shape. *J Nanotechnol* 2012; **2012**: 361853.
118. Peerakiatkhajohn P, Butburee T and Yun JH *et al.* A hybrid photoelectrode with plasmonic Au@TiO_2 nanoparticles for enhanced photoelectrochemical water splitting. *J Mater Chem A* 2015; **3**: 20127–33.
119. Teranishi M, Wada M and Naya S *et al.* Size-dependence of the activity of gold nanoparticle-loaded titanium(IV) oxide plasmonic photocatalyst for water oxidation. *Chemphyschem* 2016; **17**: 2813–7.
120. Kim HJ, Lee SH and Upadhye AA *et al.* Plasmon-enhanced photoelectrochemical water splitting with size-controllable gold nanodot arrays. *ACS Nano* 2014; **8:** 10756–65.

121. Kogo A, Takahashi Y and Sakai N *et al.* Gold cluster-nanoparticle diad systems for plasmonic enhancement of photosensitization. *Nanoscale* 2013; **5**: 7855–60.
122. Bera S, Lee JE and Rawal SB *et al.* Size-dependent plasmonic effects of Au and Au@SiO_2 nanoparticles in photocatalytic CO_2 conversion reaction of Pt/TiO_2. *Appl Catal, B* 2016; **199**: 55–63.
123. Yan J, Wu G and Guan N *et al.* Synergetic promotion of the photocatalytic activity of TiO_2 by gold deposition under UV-visible light irradiation. *Chem Commun* 2013; **49**: 11767–9.
124. Teranishi M, Hoshino R and Naya S *et al.* Gold-nanoparticle-loaded carbonate-modified titanium(IV) oxide surface: visible-light-driven formation of hydrogen peroxide from oxygen. *Angew Chem Int Ed* 2016; **55**: 12773–7.
125. Kiyonaga T, Fujii M and Akita T *et al.* Size-dependence of Fermi energy of gold nanoparticles loaded on titanium(iv) dioxide at photostationary state. *Phys Chem Chem Phys* 2008; **10**: 6553–61.
126. Kimura K, Naya S-i and Jin-nouchi Y *et al.* TiO_2 crystal form-dependence of the Au/TiO_2 plasmon photocatalyst's activity. *J Phys Chem C* 2012; **116**: 7111–7.
127. Yu J, Xiong J and Cheng B *et al.* Fabrication and characterization of Ag–TiO_2 multiphase nanocomposite thin films with enhanced photocatalytic activity. *Appl Catal B* 2005; **60**: 211–21.
128. Awazu K, Fujimaki M and Rockstuhl C *et al.* A plasmonic photocatalyst consisting of silver nanoparticles embedded in titanium dioxide. *J Am Chem Soc* 2008; **130**: 1676–80.
129. Wang P, Huang B and Qin X *et al.* Ag@AgCl: a highly efficient and stable photocatalyst active under visible light. *Angew Chem Int Ed* 2008; **47**: 7931–3.
130. Wang P, Huang B and Dai Y *et al.* Plasmonic photocatalysts: harvesting visible light with noble metal nanoparticles. *Phys Chem Chem Phys* 2012; **14**: 9813–25.
131. Lei W, Zhang T and Liu P *et al.* Bandgap- and local field-dependent photoactivity of Ag/black phosphorus nanohybrids. *ACS Catal* 2016; **6**: 8009–20.
132. Gao C, Hu Y and Wang M *et al.* Fully alloyed Ag/Au nanospheres: combining the plasmonic property of Ag with the stability of Au. *J Am Chem Soc* 2014; **136**: 7474–9.
133. Jiang R, Li B and Fang C *et al.* Metal/semiconductor hybrid nanostructures for plasmon-enhanced applications. *Adv Mater* 2014; **26**: 5274–309.
134. Wu B-H, Liu W-T and Chen T-Y *et al.* Plasmon-enhanced photocatalytic hydrogen production on Au/TiO_2 hybrid nanocrystal arrays. *Nano Energy* 2016; **27**: 412–9.
135. Weng L, Zhang H and Govorov AO *et al.* Hierarchical synthesis of non-centrosymmetric hybrid nanostructures and enabled plasmon-driven photocatalysis. *Nat Commun* 2014; **5**: 4792.
136. Jia C, Li X and Xin N *et al.* Interface-engineered plasmonics in metal/semiconductor heterostructures. *Adv Energy Mater* 2016; **6**: 1600431.